

Original article

Altered parasympathetic nervous system regulation of the sinoatrial node in Akita diabetic mice



Pooja S. Krishnaswamy^{a,1}, Emmanuel E. Egom^{a,1}, Motahareh Moghtadaei^a, Hailey J. Jansen^a, John Azer^a, Oleg Bogachev^a, Martin Mackasey^a, Courtney Robbins^a, Robert A. Rose^{a,b,*}

^a Department of Physiology and Biophysics, Dalhousie University, Halifax, Nova Scotia, Canada

^b School of Biomedical Engineering, Faculty of Medicine, Dalhousie University, Halifax, Nova Scotia, Canada

ARTICLE INFO

Article history:

Received 6 October 2014

Received in revised form 21 February 2015

Accepted 26 February 2015

Available online 6 March 2015

Keywords:

Diabetes mellitus

Sinoatrial node

Parasympathetic nervous system

Ion channels

Insulin signaling

ABSTRACT

Cardiovascular autonomic neuropathy (CAN) is a serious complication of diabetes mellitus that impairs autonomic regulation of heart rate (HR). This has been attributed to damage to the nerves that modulate spontaneous pacemaker activity in the sinoatrial node (SAN). Our objective was to test the hypothesis that impaired parasympathetic regulation of HR in diabetes is due to reduced responsiveness of the SAN to parasympathetic agonists. We used the Akita mouse model of type 1 diabetes to study the effects of the parasympathetic agonist carbachol (CCh) on SAN function using intracardiac programmed stimulation, high resolution optical mapping and patch-clamping of SAN myocytes. CCh decreased HR by 30% and increased corrected SAN recovery time (cSNRT) by 123% in wildtype mice. In contrast, CCh only decreased HR by 12%, and only increased cSNRT by 37% in Akita mice. These alterations were due to smaller effects of CCh on SAN electrical conduction and spontaneous action potential firing in isolated SAN myocytes. Voltage clamp experiments demonstrate that the acetylcholine-activated K^+ current (I_{KACH}) is reduced in Akita SAN myocytes due to enhanced desensitization and faster deactivation kinetics. These I_{KACH} alterations were normalized by treating Akita SAN myocytes with PI(3,4,5)P₃ or an inhibitor of regulator of G-protein signaling 4 (RGS4). There was no difference in the effects of CCh on the hyperpolarization-activated current (I_f) between wildtype and Akita mice. Our study demonstrates that Akita diabetic mice demonstrate impaired parasympathetic regulation of HR and SAN function due to reduced responses of the SAN to parasympathetic agonists. Our experiments demonstrate a key role for insulin-dependent phosphoinositide 3-kinase (PI3K) signaling in the parasympathetic dysfunction seen in the SAN in diabetes.

© 2015 Elsevier Ltd. All rights reserved.

1. Introduction

Cardiovascular complications are a major cause of death and morbidity in the setting of diabetes mellitus. One particularly serious complication of diabetes is cardiovascular autonomic neuropathy (CAN), which results in damage to the nerves that innervate the heart and results in abnormal autonomic regulation of heart rate (HR) [1]. CAN may affect up to 90% of diabetic patients [1] and it has been estimated that approximately 50% of individuals with diabetes for greater than 10 years display impairments in the regulation of the heart by the parasympathetic nervous system [2]. Diabetic patients with CAN display 2–5 fold increases in mortality compared to diabetic patients without CAN [1,3].

The parasympathetic nervous system modulates HR by releasing acetylcholine (ACh), which binds to muscarinic (M_2) receptors in pacemaker myocytes within the sinoatrial node (SAN) of the heart [4–6]. SAN myocytes generate spontaneous action potentials (APs) and it is the frequency of AP firing that determines HR *in vivo* [7]. The physiological basis for spontaneous APs in the SAN is the occurrence of a diastolic depolarization (DD) between successive APs during which the membrane potential slowly depolarizes from the maximum diastolic potential (MDP) until the threshold for the next AP is achieved [4,7]. Once bound to M_2 receptors, ACh modulates spontaneous AP frequency and HR by activating inhibitory G proteins (G_i), which signal *via* the α subunit (cAMP-dependent) as well as the $\beta\gamma$ subunit [4]. Several ionic currents in SAN myocytes are modulated downstream of G_i proteins including the hyperpolarization-activated current (I_f), L-type Ca^{2+} currents ($I_{Ca,L}$) and the acetylcholine-activated K^+ current (I_{KACH}). Studies using pharmacological approaches and genetically altered mice suggest that I_{KACH} is a major contributor to the HR response to ACh [8–11].

Although CAN and the impaired regulation of HR by the parasympathetic nervous system in the diabetic heart is often interpreted in the context of damage to the nerves innervating the SAN [1] we hypothesized

* Corresponding author at: Department of Physiology and Biophysics, Dalhousie University, Sir Charles Tupper Medical Building, Room 4J, 5850 College Street, PO Box 15000, Halifax B3H 4R2, Nova Scotia, Canada. Tel.: +1 902 494 2268; fax: +1 902 494 1685.

E-mail address: robert.rose@dal.ca (R.A. Rose).

¹ These authors contributed equally to this study.

that the diabetic phenotype may also be associated with intrinsic alterations in the SAN and how it responds to parasympathetic agonists. We tested this hypothesis using the Akita mouse model of type 1 diabetes [12,13]. Akita mice are characterized by a mutation in the insulin-2 (*Ins2*) gene that results in severe pancreatic β cell dysfunction, which prevents insulin release and thus leads to development of the diabetic phenotype including hypoinsulinemia and hyperglycemia [14]. Akita mice have been shown to replicate many diabetic complications, including neuropathy; thus, this model represents an excellent model of human diabetes [14]. Our data demonstrate that Akita diabetic mice are characterized by alterations in parasympathetic regulation of HR due to a reduction in the responsiveness of the SAN to parasympathetic agonists in association with impaired insulin-dependent signaling in SAN myocytes.

2. Methods

An expanded Methods section is available in the Supplementary data.

2.1. Animals

This study utilized littermate wildtype and type 1 diabetic Akita mice between the ages of 16 and 20 weeks. Progression of diabetes (genotyping) was determined by assessing urine glucose, protein and ketones (using keto-diastix reagent strips for urinalysis) as well as serum glucose levels (using a glucometer).

In some experiments Akita mice were treated with insulin (or placebo) for 4 weeks beginning at 12 weeks of age. This was done by implanting insulin or placebo pellets (LinShin Canada, Inc.) subcutaneously. In all studies (*in vivo* and isolated preparations) temperature was controlled and therefore not different between wildtype and Akita mice. All experimental procedures were approved by the Dalhousie University Committee for Laboratory Animals and conformed to the guidelines of the Canadian Council on Animal Care.

2.2. Echocardiography

Transthoracic echocardiography was performed on anesthetized mice (1% isoflurane inhalation) using a 14 MHz transducer and a GE Vivid 7 ultrasound machine as we have done previously [15]. Cardiac structure and function were assessed by measuring 2 dimensional M-mode images from the parasternal short axis at the level of the midpapillary muscle and the parasternal long axis.

2.3. *In vivo* electrophysiology and programmed stimulation

Surface ECGs (used to assess changes in heart rate) were measured in anesthetized mice (2% isoflurane inhalation) using 30 gauge subdermal needle electrodes (Grass Technologies). A 1.2 French octapolar electrophysiology catheter was inserted into the right heart *via* the jugular vein and used for intracardiac pacing experiments. Sinoatrial node recovery time (SNRT) was measured by delivering a 12 stimulus drive train at a cycle length of 100 ms and measuring the latency to the first spontaneous P wave, as we have described previously [15].

2.4. High resolution optical mapping

To study patterns of electrical conduction in the SAN we used high resolution optical mapping in atrial preparations (Supplemental Fig. 4) as we have done previously [15,16]. Optical mapping was done using the voltage sensitive dye di-4-ANEPPS (10 μ M). Blebbistatin (10 μ M) was added to the superfusate to suppress contractile activity. All analyses were performed using custom software. Details are provided in the Supplementary data.

2.5. Patch-clamping of sinoatrial node myocytes

SAN myocytes were isolated from wildtype and Akita mice enzymatically as we have described previously [17–19]. These SAN myocytes were used to measure spontaneous APs using the perforated patch-clamp technique as well as I_{KACH} and I_f currents using the whole-cell patch-clamp technique. The solutions and experimental protocols for these measurements are described in the Supplementary data.

2.6. Quantitative PCR

Quantitative gene expression in SAN, as well as right and left atrial samples, was performed as we have described previously [17,19]. Intron spanning primers were designed for collagen I (*col1a*), and Collagen III (*col3a*), RGS4, HCN4, ANP, β -actin (*Actb*) and GAPDH. HCN4 and ANP expression were used to distinguish SAN from right atrial samples [17,19]. Experimental protocols are described in the Supplementary data.

2.7. Collagen staining

To assess collagen deposition we used picosirius red (collagen) and fast green (healthy myocardium) staining of paraffin embedded sections (5 μ M) through the right and left atrial appendages. The level of fibrosis was quantified using ImageJ software.

2.8. Statistical analysis

All data are presented as means \pm SEM. Data were analyzed using either a Student's *t*-test or one or two way ANOVA with Tukey's posthoc test. $P < 0.05$ was considered significant.

3. Results

3.1. Cardiac structure in Akita diabetic mice

Consistent with prior studies [20–22], we found that Akita diabetic mice are characterized by clear hyperglycemia at 16–20 weeks of age (33.5 ± 2.2 mM) compared to age matched wildtype littermates (7.5 ± 0.4 mM; $P < 0.05$; Supplemental Fig. 1). Body mass was reduced ($P < 0.05$) in Akita mice compared to wildtype littermates (Supplemental Fig. 1) as previously described [20].

We assessed cardiac structure and function in Akita and wildtype mice using echocardiography. These data demonstrate that left atrial diameter and the left atria/aorta ratio were slightly increased ($P < 0.05$) in Akita mice compared to wildtypes (Supplemental Fig. 2, Supplemental Table 1). No differences were seen in the thickness of the interventricular septum ($P = 0.081$) or the left ventricular posterior wall ($P = 0.481$) and there were no differences in left ventricular internal diameter ($P = 0.06$); however ejection fraction and fractional shortening were also modestly increased ($P < 0.05$) while heart rate was reduced ($P < 0.05$) in Akita mice (Supplemental Table 1).

3.2. Altered parasympathetic regulation of the sinoatrial node in Akita diabetic mice

Akita mice have been shown to display abnormal heart rate responses to parasympathetic nervous system agonists [21]; however, direct measures of SAN function during parasympathetic activation have not been performed. Accordingly, we began by studying the effects of CCh (0.1 mg/kg; IP injection) on HR and cSNRT in anesthetized mice (Fig. 1A). Measurements of cSNRT enable direct assessment of SAN function in different conditions *in vivo* [23,24]. The effects of CCh were assessed 10 min after injection, when the effects of CCh are at a stable maximum. These experiments demonstrate that CCh reduced ($P < 0.05$) HR in wildtype and Akita mice (Fig. 1B); however,

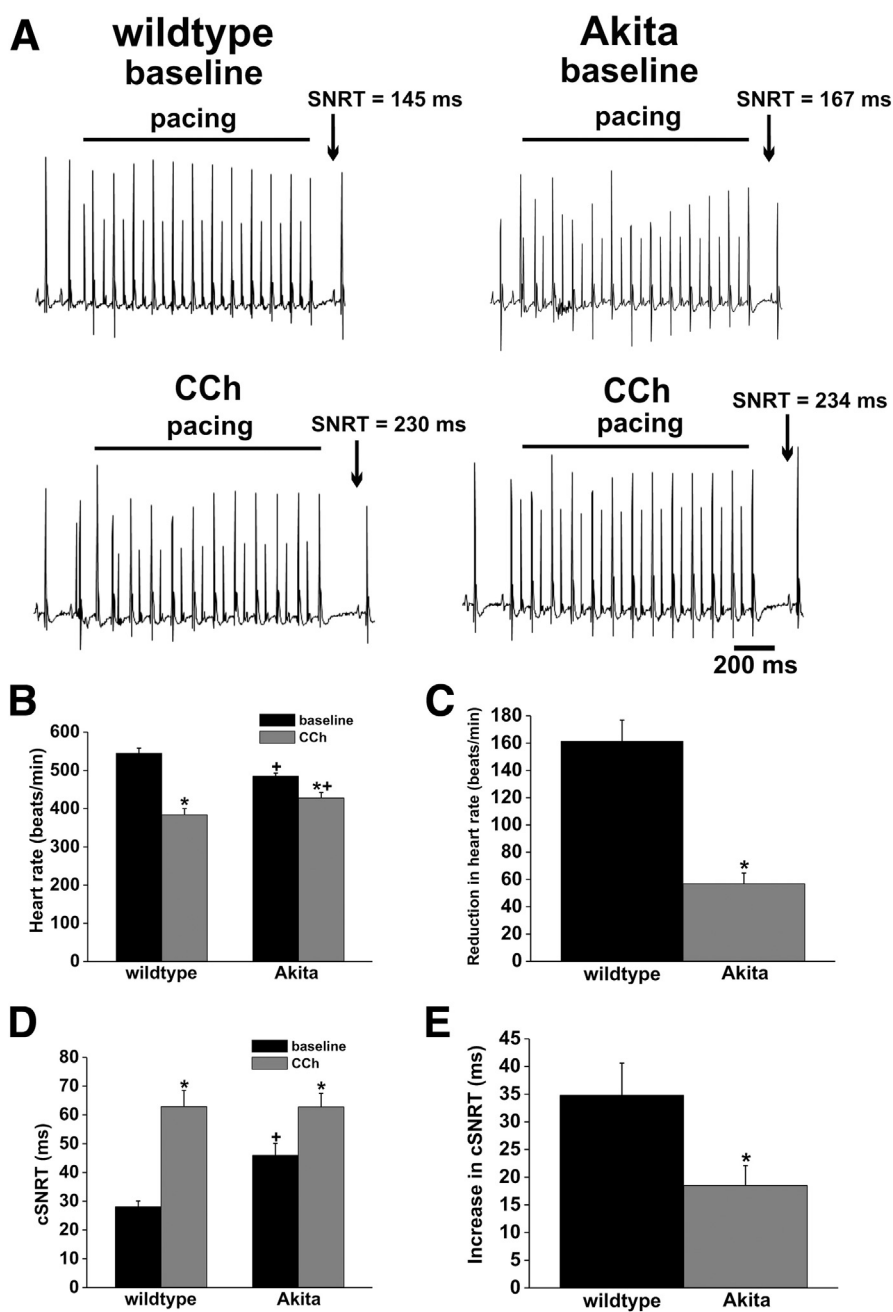


Fig. 1. Effects of carbachol on heart rate and sinoatrial node function in Akita diabetic mice *in vivo*. (A) Representative ECG recordings illustrating assessment of sinoatrial node recovery time (SNRT) under baseline conditions and after intraperitoneal injection of CCh (0.1 mg/kg) in anesthetized wildtype and Akita diabetic mice. (B) Summary data illustrating the effects of CCh on HR in wildtype ($n = 9$) and Akita ($n = 10$) mice. * $P < 0.05$ vs. baseline; + $P < 0.05$ vs. wildtype. Data analyzed by two way ANOVA with Tukey's posthoc test. (C) Summary data illustrating the magnitude of the reduction in HR elicited by CCh in wildtype and Akita mice. * $P < 0.05$ vs. wildtype by Student's t -test. (D) Summary data illustrating the effects of CCh on SNRT after correcting for HR (cSNRT) in wildtype ($n = 9$) and Akita ($n = 10$) mice. * $P < 0.05$ vs. baseline; + $P < 0.05$ vs. wildtype. Data analyzed by two way ANOVA with Tukey's posthoc test. (E) Summary data illustrating the magnitude of the increase in cSNRT elicited by CCh in wildtype and Akita mice. * $P < 0.05$ vs. wildtype by Student's t -test.

quantification of the magnitude of the effect of CCh (Fig. 1C) demonstrates that CCh was less effective ($P < 0.05$) in Akita mice. Consistent with these HR changes, CCh increased cSNRT in wildtype and Akita mice (Fig. 1D); however, the magnitude of the increase in cSNRT was reduced ($P < 0.05$) in Akita mice (Fig. 1E). In agreement with a prior study of SAN function in diabetes [25] the data in Fig. 1 show that HR in Akita mice was also lower at baseline in association with a prolonged cSNRT.

We also measured the effects of CCh (1 μ M) on HR in isolated Langendorff-perfused hearts where HR is determined by intrinsic SAN function independently of the autonomic nervous system (Fig. 2). Consistent with the *in vivo* studies described above, HR was lower ($P < 0.05$) at baseline in Akita mice. CCh reduced ($P < 0.05$) HR in wildtype and

Akita hearts (Fig. 2B); however, once again, the magnitude of this reduction was smaller ($P < 0.05$) in Akita hearts (Fig. 2C). Collectively, the data in Figs. 1 and 2 demonstrate that, even accounting for baseline differences, HR was elevated ($P < 0.05$) in Akita mice following application of CCh due to a reduced responsiveness of the SAN to CCh.

3.3. Effects of carbachol on sinoatrial node function in Akita mice treated with insulin

To determine the role of insulin in altered parasympathetic regulation of the SAN in diabetes, Akita mice were implanted with insulin pellets (or placebo) for 4 weeks. Following this, the effects of CCh

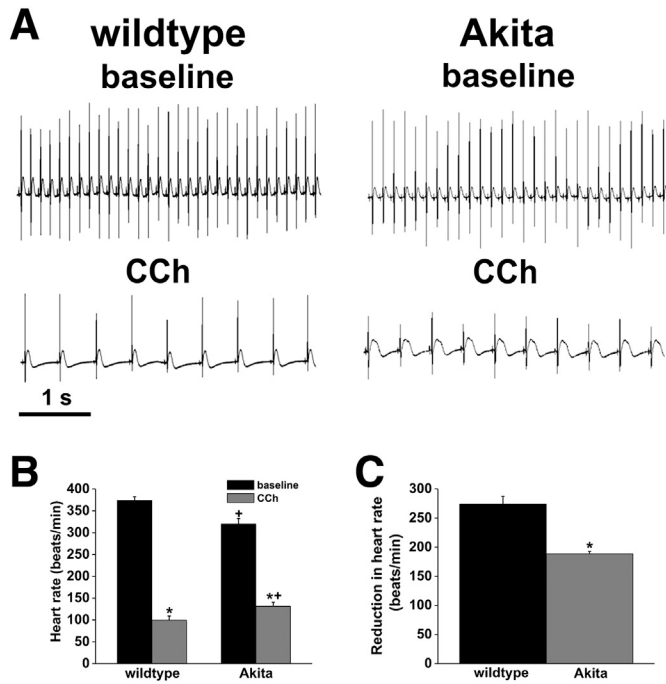


Fig. 2. Effects of carbachol on heart rate in isolated hearts from wildtype and Akita mice. (A) Representative ECG recordings from isolated Langendorff-perfused hearts under baseline conditions and after application of CCh (1 μ M). (B) Summary data illustrating the effects of CCh on HR in wildtype ($n = 5$) and Akita ($n = 5$) hearts. * $P < 0.05$ vs. baseline; † $P < 0.05$ vs. wildtype. Data analyzed by two way ANOVA with Tukey's posthoc test. (C) Summary data illustrating the magnitude of the reduction in HR elicited by CCh in wildtype and Akita hearts. * $P < 0.05$ vs. wildtype by Student's t -test.

(0.1 mg/kg, IP injection) on HR and cSNRT were evaluated *in vivo* (Fig. 3). Insulin treatment reduced blood glucose in Akita mice to 13.3 ± 1.9 mM whereas blood glucose remained elevated (39.9 ± 2.1 mM; $P < 0.05$) in placebo treated Akita mice (Supplemental Fig. 3). CCh elicited larger effects on HR and cSNRT in insulin treated Akita mice compared to placebo controls (Figs. 3B and D). Overall, the reduction in HR elicited by CCh was increased ($P < 0.05$) from 78 ± 20 beats/min in placebo to 169 ± 16 beats/min following insulin treatment (Fig. 3C) while the magnitude of the increase in cSNRT elicited by CCh was increased from 14.3 ± 2.3 ms to 31.2 ± 3 ms (Fig. 3E). Collectively, the data in Fig. 3 demonstrate that insulin treatment in Akita mice corrected the baseline differences in HR and cSNRT and increased the magnitude of the responses to CCh to values very similar to wildtype mice.

3.4. Impaired effects of carbachol on electrical conduction in the sinoatrial node in Akita mice

To begin to understand the mechanisms for the impaired responsiveness of the SAN to parasympathetic agonists, we used high resolution optical mapping to assess the effects of CCh (0.1 μ M) on electrical conduction in the SAN in wildtype and Akita mice. These experiments were performed in intact atrial preparations (Supplemental Fig. 4) in which we can map electrical propagations from the SAN within the right atrial posterior wall, as we have described previously [15,16]. Consistent with our prior work [15,16], representative activation maps (Fig. 4A) illustrate that in baseline conditions the first electrical breakthrough occurs in the right atrial posterior wall, adjacent to the crista terminalis and closer to the opening of the superior vena cava. Application of CCh results in a slowing of conduction in wildtype and Akita mice (note the increased number of isochrones and less spacing between adjacent isochrones in the presence of CCh); however the effect was clearly smaller in Akita hearts. Activation maps from wildtype mice

also demonstrate that, consistent with prior studies [26,27], CCh slows conduction in association with a shift in the leading pacemaker site in the inferior direction within the right atrial posterior wall. The locations of the leading pacemaker site in basal conditions and after application of CCh in wildtype and Akita mice are demonstrated for each heart studied in Fig. 4B. This assessment clearly demonstrates that CCh induced an inferior shift in the leading pacemaker site in all hearts; however, the magnitude of the shift was reduced ($P < 0.05$) in Akita hearts (0.77 ± 0.2 mm) compared to wildtypes (2.55 ± 0.23 mm; Fig. 4C).

This first set of optical mapping studies was performed using atrial preparations in sinus rhythm where the intrinsic cycle length was free to change. CCh increased ($P < 0.05$) cycle length (corresponds to a decrease in HR) in wildtype and Akita hearts (Fig. 4D); however, consistent with the data described in Figs. 1 and 2, the increase in cycle length elicited by CCh was smaller ($P < 0.05$) in Akita hearts (Fig. 4E). We also determined the effects of CCh on local conduction velocity (CV) in the region of the leading pacemaker site within the SAN (Fig. 4F). Note that in all cases these CVs are very low (*i.e.* less than 10 cm/s) as expected for the SAN [16,26,28,29]. As illustrated in Fig. 4G the reduction in CV elicited by CCh in Akita mice was reduced ($P < 0.05$) compared to wildtype hearts. Because CV can be dependent on cycle length, we also studied the effects of CCh on SAN CV in atrial preparations paced at a fixed cycle length of 120 ms. In these experiments the effects of CCh on SAN CV were comparable to those shown in sinus rhythm and the ability of CCh to slow SAN CV was still reduced in Akita hearts (data not shown). Together, these data demonstrate that the effects of CCh on electrical conduction in the SAN are significantly impaired in Akita mice. Consistent with our *in vivo* findings, these optical mapping studies also show that cycle length was longer and SAN CV was reduced in Akita hearts at baseline.

Finally, we measured optical APs from the region of the leading pacemaker site in wildtype and Akita hearts in baseline conditions and after application of CCh (Supplemental Fig. 5). As expected for the SAN, these optical APs are characterized by the presence of a distinct DD between successive APs. These representative recordings illustrate that CCh increased the cycle length of spontaneous AP firing in association with a reduction in DD slope in wildtype mice. These effects of CCh on SAN APs were noticeably reduced in Akita hearts.

3.5. Effects of carbachol on spontaneous action potential firing in isolated sinoatrial node myocytes in Akita diabetic mice

Next, we used isolated SAN myocytes from wildtype and Akita mice to study the effects of CCh (0.1 μ M) on spontaneous AP firing patterns in more detail (Fig. 5A; Supplemental Table 2). Consistent with the optical AP data described above, CCh reduced spontaneous AP firing frequency in wildtype and Akita SAN myocytes, but the effect was reduced ($P < 0.05$) in Akita mice (Fig. 5B). Similarly, CCh decreased the DD slope (Fig. 5C) and hyperpolarized the MDP (Fig. 5D) to a smaller extent ($P < 0.05$) in Akita SAN myocytes. On the other hand, the AP take-off potential was not affected by CCh and did not differ between Akita and wildtype mice (Supplemental Table 2). The effects of CCh on SAN AP firing were completely reversible upon washout (Figs. 5B–D).

Interestingly, despite the baseline differences in heart rate, cSNRT and electrical conduction measured *in vivo* and in isolated hearts/atrial preparations, we observed no baseline differences in AP frequency ($P = 0.264$), DD slope ($P = 0.419$) or MDP ($P = 0.253$) in isolated SAN myocytes from wildtype and Akita mice (Figs. 5B–4D). This is consistent with a prior study showing that type 1 diabetic mice (streptozotocin model) have SAN dysfunction due to fibrosis in the SAN and apoptosis of SAN myocytes rather than differences in AP firing in isolated SAN myocytes [25]. To determine if Akita mice are similarly characterized by enhanced fibrosis we assessed mRNA expression of collagens I and III in the SAN and atria as well as patterns of interstitial fibrosis in the atria using picrosirius red staining. These data

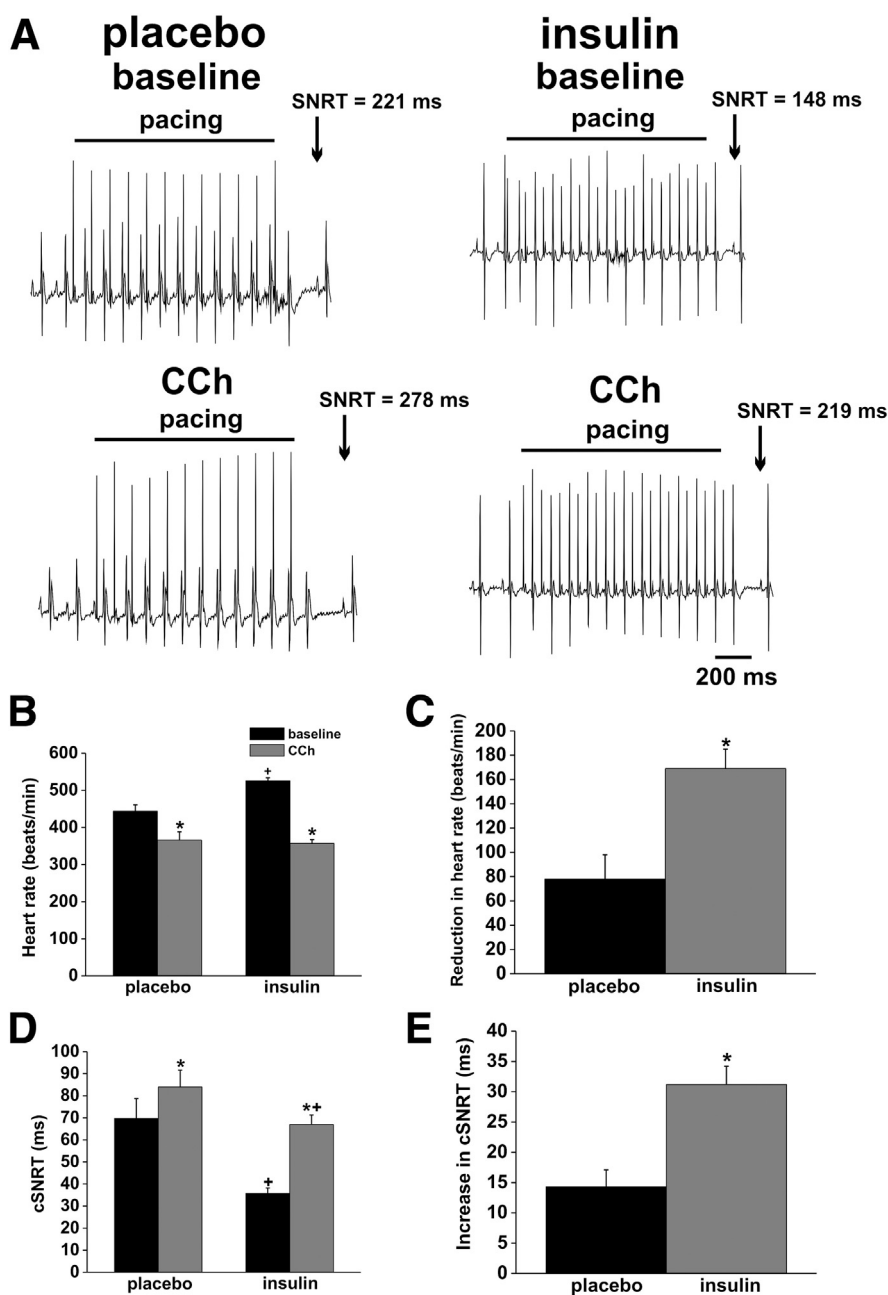


Fig. 3. Effects of carbachol on heart rate and sinoatrial node function in Akita mice treated with insulin. Akita mice were implanted with insulin pellets or placebo for 4 weeks prior to assessment of HR and SNRT. (A) Representative ECG recordings illustrating assessment of sinoatrial node recovery time (SNRT) under baseline conditions and after intraperitoneal injection of CCh (0.1 mg/kg) in Akita diabetic mice treated with placebo or insulin. (B) Summary data illustrating the effects of CCh on HR in Akita mice treated with placebo ($n = 4$) or insulin pellets ($n = 6$). * $P < 0.05$ vs. baseline; [†] $P < 0.05$ vs. placebo. Data analyzed by two way ANOVA with Tukey's posthoc test. (C) Summary data illustrating the magnitude of the reduction in HR elicited by CCh in Akita mice treated with placebo or insulin pellets. * $P < 0.05$ vs. placebo by Student's t -test. (D) Summary data illustrating the effects of CCh on cSNRT in Akita mice treated with placebo ($n = 4$) or insulin pellets ($n = 6$). * $P < 0.05$ vs. baseline; [†] $P < 0.05$ vs. placebo. Data analyzed by two way ANOVA with Tukey's posthoc test. (E) Summary data illustrating the magnitude of the increase in cSNRT elicited by CCh in Akita mice treated with placebo or insulin pellets. * $P < 0.05$ vs. placebo by Student's t -test.

demonstrate that the expression of collagen I and collagen III are both increased ($P < 0.05$) in the SAN, right atrium and left atrium of Akita mice compared to wildtypes (Supplemental Fig. 6). Consistent with this, we found that interstitial fibrosis was greater ($P < 0.05$) in the atria of Akita mice compared to wildtype controls (Supplemental Fig. 7). We also performed picrosirius red staining on Akita atria following 4 weeks of insulin treatment and found that interstitial fibrosis was reduced ($P < 0.05$) compared to untreated Akita wildtype mice (Supplemental Fig. 7). Specifically, insulin treated Akita mice showed levels of right and left atrial fibrosis that were not different from wildtypes.

3.6. I_{KACH} is altered in SAN myocytes from Akita diabetic mice

The observation that impaired parasympathetic modulation of AP firing in SAN myocytes of Akita mice is associated with altered effects of CCh on MDP as well as DD slope suggests an important role for I_{KACH} in these responses. This is because I_{KACH} plays a key role in hyperpolarizing the MDP during parasympathetic activation, which can lead to alterations in the DD [4,10]. Accordingly, we next investigated the properties of I_{KACH} in SAN myocytes from wildtype and Akita mice (Fig. 6). Representative recordings (Fig. 6A) illustrate the effects of CCh (10 μ M) on inward I_{KACH} current at -100 mV. Consistent with

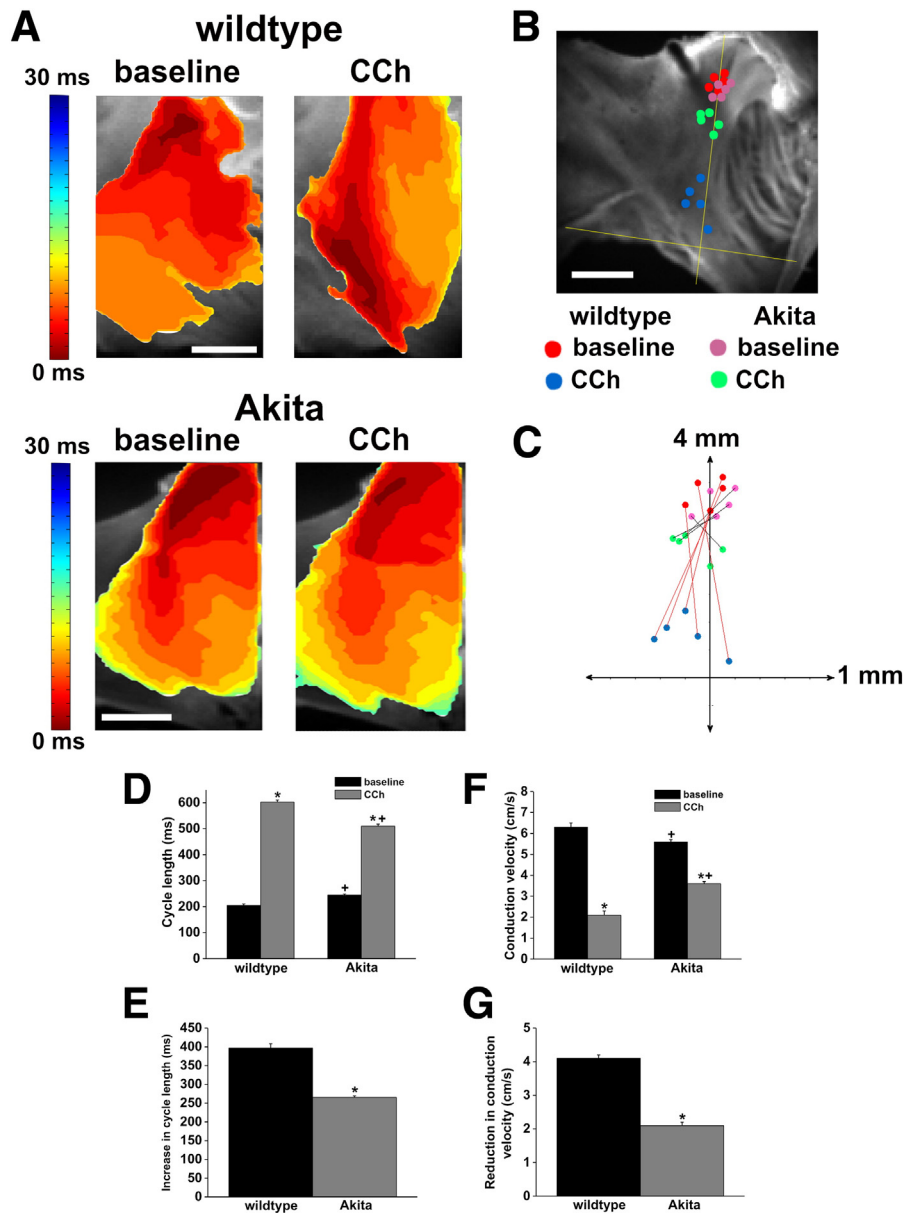


Fig. 4. Effects of CCh on patterns of electrical conduction in the sinoatrial node in Akita diabetic mice. (A) Representative color maps showing activation patterns in baseline conditions and after application of CCh (0.1 μ M) in atrial preparations from wildtype and Akita mice (see also Supplemental Fig. 4). Red color indicates earliest activation time in the sinoatrial node within the right atrial posterior wall. Time interval between isochrones is 1.8 ms. Scale bars are 1 mm. (B) Location of the leading pacemaker site within the right atrial posterior wall in baseline conditions and following application of CCh in wildtype and Akita hearts. Color scheme for each circle is the same as in panel B. (C) Quantification of the magnitude of the shift in the leading pacemaker site in baseline conditions and following application of CCh in wildtype and Akita hearts. Color scheme for each circle is the same as in panel B. (D) Summary of the effects of CCh on cycle length in atrial preparations from wildtype ($n = 5$) and Akita ($n = 5$) mice. * $P < 0.05$ vs. baseline; + $P < 0.05$ vs. wildtype. Data analyzed by two way ANOVA with Tukey's posthoc test. (E) Summary data illustrating the magnitude of the increase in cycle length elicited by CCh in wildtype and Akita mice. * $P < 0.05$ vs. wildtype by Student's t -test. (F) Summary of the effects of CCh on SAN conduction velocity during normal sinus rhythm in wildtype and Akita mice. * $P < 0.05$ vs. baseline; + $P < 0.05$ vs. wildtype. Data analyzed by two way ANOVA with Tukey's posthoc test. (G) Summary data illustrating the magnitude of the reduction in SAN conduction velocity elicited by CCh during normal sinus rhythm. * $P < 0.05$ vs. wildtype by Student's t -test.

previously published results, these recordings demonstrate that CCh potently activates an inward I_{KACH} , which then undergoes a process of desensitization during which I_{KACH} decreases in the continued presence of CCh [30,31]. Upon removal of CCh, I_{KACH} deactivates and inward current returns to basal levels. Summary data demonstrate that I_{KACH} desensitization is enhanced (Fig. 6B; $P < 0.05$) and that the effects of CCh reverse faster (Fig. 6C; $P < 0.05$) in Akita SAN myocytes. These alterations are also evident from I_{KACH} I-V relationships (Figs. 6D and E), which show reductions in Akita mice only after the desensitization process has taken place. In contrast, the I_{KACH} I-V relationships at the peak of the CCh response were not different ($P = 0.427$) between genotypes.

To further assess the properties of I_{KACH} in Akita SAN myocytes we studied the dose dependence of the effects of CCh on this current (Supplemental Fig. 8). These experiments show that the peak amplitude of I_{KACH} (i.e. before desensitization) is not different between wildtype and Akita SAN myocytes at CCh doses between 0.1 and 100 μ M. On the other hand, I_{KACH} desensitization was consistently greater ($P < 0.05$) in Akita SAN myocytes at all CCh doses tested. Together these data clearly demonstrate that reduced parasympathetic responses in SAN myocytes occur in association with smaller I_{KACH} due to alterations in the desensitization and deactivation kinetics of I_{KACH} .

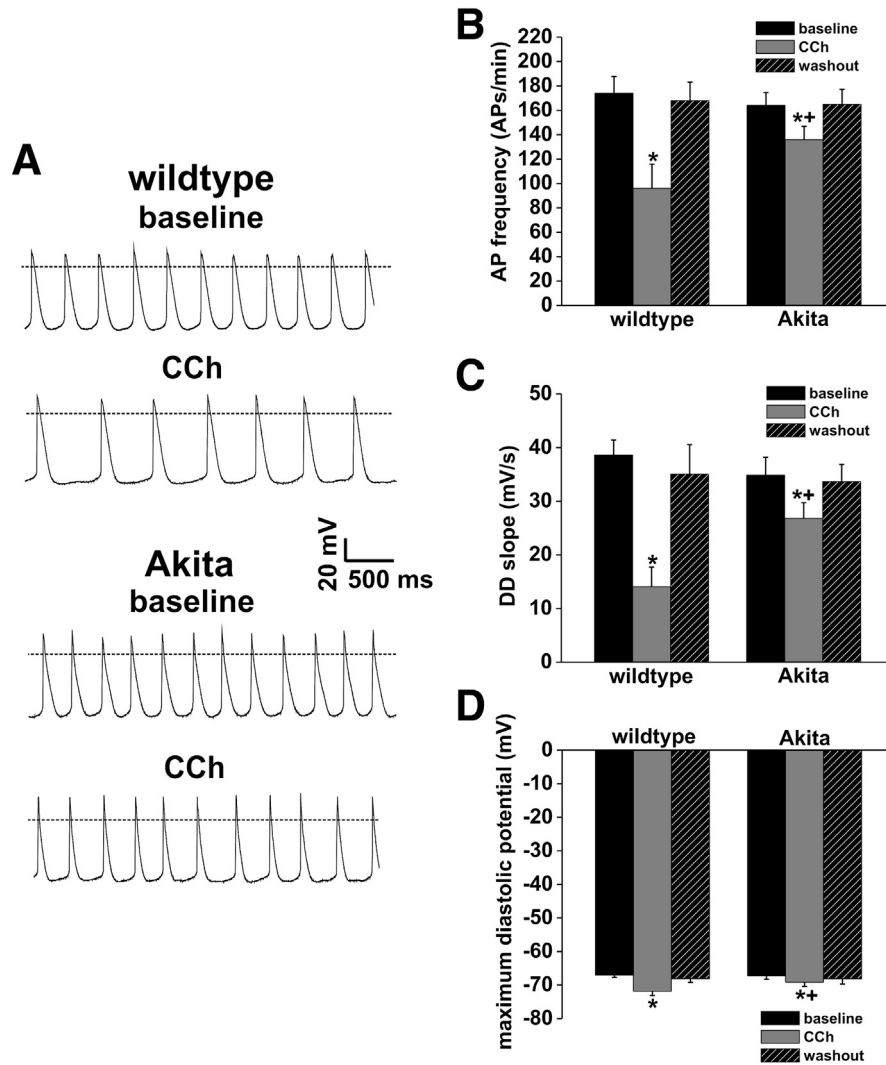


Fig. 5. Effects of carbachol on spontaneous action potential firing in isolated sinoatrial node myocytes from Akita diabetic mice. (A) Representative spontaneous APs in baseline conditions and after application of CCh (0.1 μ M) in SAN myocytes from wildtype and Akita mice. (B) Summary of the effects of CCh on spontaneous AP frequency in wildtype and Akita SAN myocytes. (C) Summary of the effects of CCh on DD slope in wildtype and Akita SAN myocytes. (D) Summary of the effects of CCh on MDP in wildtype and Akita SAN myocytes. * $P < 0.05$ vs. baseline; + $P < 0.05$ vs. wildtype. Data analyzed by two way ANOVA with Tukey's posthoc test; $n = 7$ wildtype and 7 Akita SAN myocytes.

To determine whether other ionic currents show altered parasympathetic responsiveness in Akita SAN myocytes we measured the effects of CCh (10 μ M) on I_f (Supplemental Fig. 9). These data demonstrate that, in contrast to $I_{K_{ACh}}$, CCh reduced I_f density to a very similar extent in wildtype and Akita SAN myocytes. There was no difference ($P = 0.11$) in the effectiveness of CCh on I_f in Akita mice. Furthermore, consistent with the absence of a difference in baseline spontaneous AP firing frequency, there was no difference ($P = 0.36$) in basal I_f density in wildtype and Akita mice.

3.7. Phosphatidylinositol (3,4,5) P_3 reverses the impairments in $I_{K_{ACh}}$ in Akita diabetic mice

Our *in vivo* studies demonstrate that treating Akita mice with insulin reverses the alterations in parasympathetic regulation of the SAN in the diabetic heart suggesting that a loss of insulin signaling plays a key role in this response. A major mechanism by which insulin mediates its effects is through PI3K signaling, which generates phosphatidylinositol (3,4,5) P_3 (PIP₃), a phospholipid that modulates several downstream signaling molecules [32]. The absence of insulin in Akita mice would reduce the production of PIP₃ and this could account for the observed impairments in parasympathetic modulation

of $I_{K_{ACh}}$ in the diabetic heart. To test this hypothesis we infused wildtype and Akita SAN myocytes with PIP₃ (1 μ M) for 5 min *via* the recording pipette and then measured the properties of $I_{K_{ACh}}$ during application of CCh (10 μ M). Representative recordings (Fig. 7A) and summary data (Figs. 7B and C) demonstrate that $I_{K_{ACh}}$ desensitization ($P = 0.857$) and recovery time ($P = 0.352$) were no longer different between wildtype and Akita SAN myocytes following intracellular application of PIP₃.

To confirm a specific role for PIP₃ we also treated wildtype and Akita SAN myocytes with another phospholipid, phosphatidylinositol 4,5-bisphosphate (PIP₂; also delivered *via* the recording pipette), which is not a direct mediator of the effects of PI3K [32]. These data (Figs. 7D–F) demonstrate that $I_{K_{ACh}}$ desensitization remained greater ($P < 0.05$) and $I_{K_{ACh}}$ recovery remained faster ($P < 0.05$) in PIP₂ treated Akita SAN myocytes compared to wildtype. Together these data demonstrate that treatment with PIP₃ abolishes the differences in $I_{K_{ACh}}$ between wildtype and Akita SAN myocytes.

3.8. RGS4 inhibition normalizes $I_{K_{ACh}}$ in Akita diabetic SAN myocytes

Our data demonstrate that a key component of the impaired parasympathetic regulation of the heart in Akita mice is the enhanced

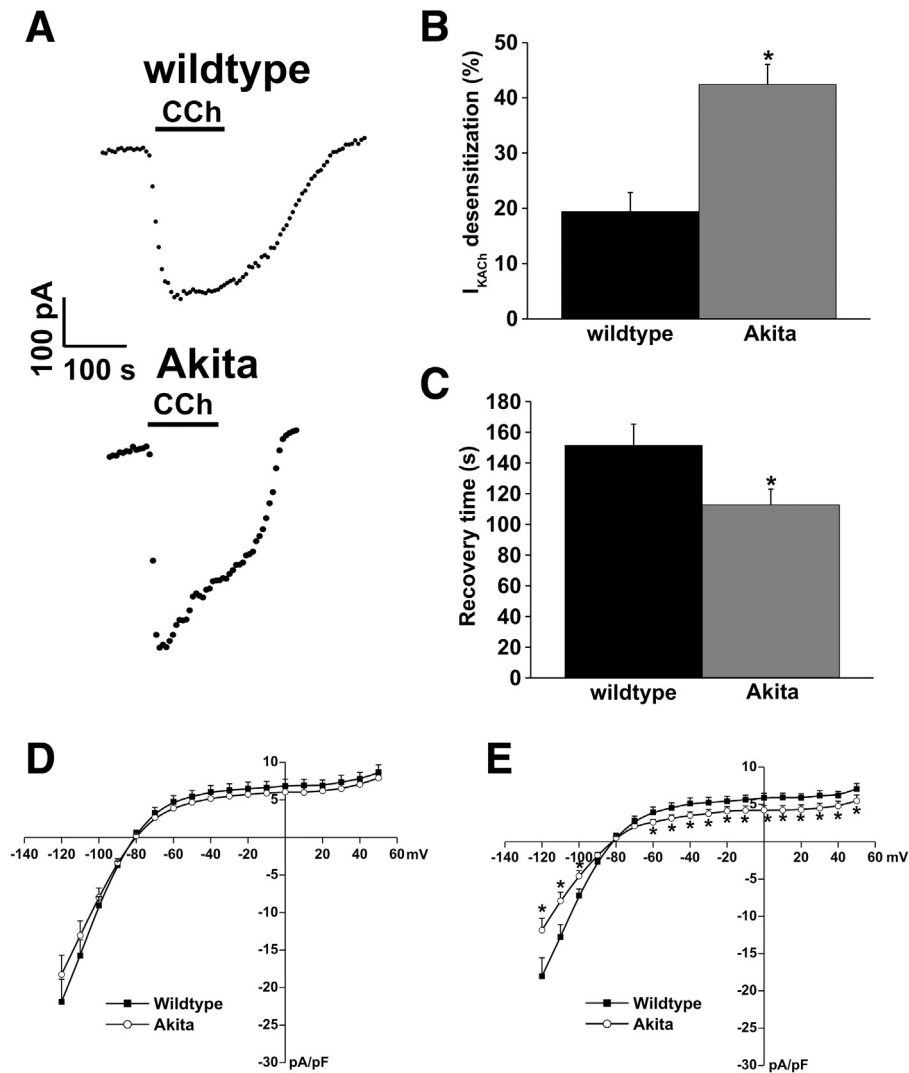


Fig. 6. Comparison of $I_{K_{ACh}}$ kinetics and current density in SAN myocytes from Akita mice. (A) Time course of the effects of CCh (10 μ M) on inward $I_{K_{ACh}}$ measured at -100 mV in wildtype and Akita SAN myocytes. Note that $I_{K_{ACh}}$ amplitude decreases (desensitization) in the continued presence of CCh. Time scale is the same for both recordings. (B) Summary data illustrating the extent of $I_{K_{ACh}}$ desensitization in wildtype and Akita SAN myocytes. (C) Summary data illustrating the recovery time for washoff of CCh in wildtype and Akita SAN myocytes. * $P < 0.05$ vs wildtype by Student's t -test for panels B and C; $n = 11$ wildtype and 15 Akita SAN myocytes. (D) $I_{K_{ACh}}$ I-V relationships in wildtype and Akita SAN myocytes measured at the peak of the response to CCh. There was no significant difference in peak $I_{K_{ACh}}$ density in SAN myocytes between genotypes ($P = 0.427$). (E) $I_{K_{ACh}}$ I-V relationships in wildtype and Akita SAN myocytes measured 2 min after application of CCh when desensitization has occurred. $P < 0.05$ vs. wildtype by Student's t -test at each membrane potential. For panels D and E $n = 11$ wildtype and 15 Akita SAN myocytes.

desensitization and deactivation kinetics of $I_{K_{ACh}}$ in the SAN. We have recently demonstrated that regulator of G protein signaling 4 (RGS4) is a critical regulator of $I_{K_{ACh}}$ desensitization and deactivation during parasympathetic signaling in the SAN [31]. Furthermore, RGS4 is known to be inhibited by PIP_3 [33,34]. Thus, we hypothesized that the absence of insulin would result in greater RGS4 activity in Akita mice due to the loss of insulin dependent inhibition of RGS4 by PIP_3 . To test this hypothesis we treated wildtype and Akita SAN myocytes with a selective RGS4 inhibitor, CCG-4986 (10 μ M) [35,36], which was dialyzed into cells via the recording pipette before the effects of CCh (10 μ M) were studied (Fig. 8). These data demonstrate that CCG-4986 reduced $I_{K_{ACh}}$ desensitization and prolonged $I_{K_{ACh}}$ deactivation in wildtype and Akita SAN myocytes (Figs. 8B and C) and abolished any $I_{K_{ACh}}$ differences between these two groups of mice. Following RGS4 inhibition with CCG-4986, there were no differences in $I_{K_{ACh}}$ desensitization ($P = 0.928$) or recovery time ($P = 0.712$) between wildtype and Akita SAN myocytes. Quantitative PCR revealed no significant differences in the expression of RGS4 in the SAN (or atria) of Akita mice compared to wildtypes (Supplemental Fig. 10).

4. Discussion

In this study we used the Akita mouse model of type 1 diabetes to investigate whether altered parasympathetic regulation of HR, which occurs in diabetic patients [1], involves changes in how the SAN responds to parasympathetic agonists. Our measurements of the effects of CCh on HR and cSNRT *in vivo* as well as in isolated hearts demonstrate that Akita mice recapitulate the reduced parasympathetic regulation of HR seen in diabetics and further demonstrate that this is due, at least in part, to changes in the responsiveness of the SAN to CCh. Although autonomic regulation of HR *in vivo* involves the sympathetic and parasympathetic nervous systems, both of which could be altered in diabetes [1,37], our experiments in isolated hearts (where HR is determined only intrinsic SAN function) clearly support the conclusion that responsiveness of the SAN to parasympathetic nervous system agonists is reduced in Akita mice. It should be noted that the reductions in heart rate observed in isolated hearts were larger than those seen *in vivo*. This is likely the result of different concentrations of CCh used in the two experiments as well as the fact that in the Langendorff study CCh was perfused

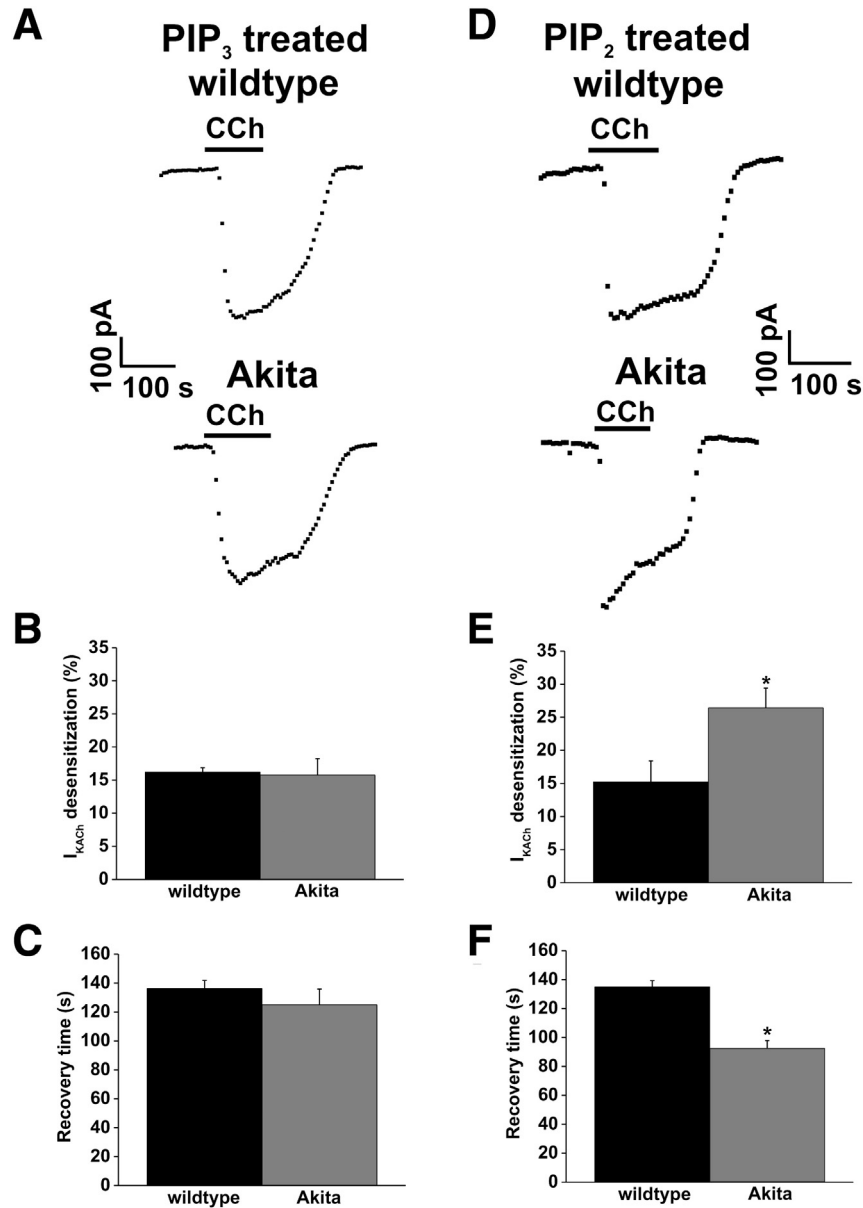


Fig. 7. Kinetic properties of $I_{K_{ACh}}$ in SAN myocytes from Akita mice treated with PIP_3 or PIP_2 . In these experiments PIP_3 (1 μM) or PIP_2 (1 μM) were included in the recording pipette and dialyzed into SAN myocytes for 5 min before the effects of CCh (10 μM) were studied. (A) Representative time course recordings illustrating the kinetic properties of $I_{K_{ACh}}$ measured at -100 mV in wildtype and Akita SAN myocytes treated with PIP_3 . Scale bars are identical for both recordings. (B) Summary data illustrating the extent of $I_{K_{ACh}}$ desensitization in wildtype and Akita SAN myocytes treated with PIP_3 . (C) Summary data illustrating the time course of recovery of $I_{K_{ACh}}$ to baseline in wildtype and Akita SAN myocytes treated with PIP_3 . There were no differences in $I_{K_{ACh}}$ desensitization ($P = 0.857$) or recovery time ($P = 0.352$) between wildtype and Akita SAN myocytes following PIP_3 treatment. Data analyzed by Student's t -test; $n = 5$ wildtype and 6 Akita SAN myocytes. (D) Representative time course recordings illustrating the kinetic properties of $I_{K_{ACh}}$ measured at -100 mV in wildtype and Akita SAN myocytes treated with PIP_2 . Scale bars are identical for both recordings. (E) Summary data illustrating the extent of $I_{K_{ACh}}$ desensitization in wildtype and Akita SAN myocytes treated with PIP_2 . (F) Summary data illustrating the time course of recovery of $I_{K_{ACh}}$ to baseline in wildtype and Akita SAN myocytes treated with PIP_2 . * $P < 0.05$ vs. wildtype by Student's t -test; $n = 5$ wildtype and 5 Akita SAN myocytes.

directly into the heart while in anesthetized mice CCh was delivered systemically by intraperitoneal injection. It is also possible that the presence of an intact sympathetic nervous system impacts the magnitude of the CCh effect *in vivo*, but not in the isolated heart. These findings demonstrate that impaired parasympathetic regulation of HR in diabetes is due to alterations in the intrinsic signaling pathways activated by parasympathetic agonists within the SAN, in addition to the possibility of damage to the nerves innervating the SAN (*i.e.* neuropathy), which has been previously implicated [1].

A major mechanism by which CCh slows HR is by slowing electrical conduction within the SAN [26,27]. Furthermore, It is well established that this slowing of electrical conduction in the SAN is associated with an inferior shift in the leading pacemaker site [26,27,38]. In wildtype

mice we consistently observed this inferior shift in the leading pacemaker site and the magnitude of this shift was very similar to that previously reported in mice [27]. In contrast, the magnitude of the shift in the leading pacemaker site following application of CCh was profoundly reduced in Akita mice. This is the first indication that the shifting of the leading pacemaker site in the presence of parasympathetic agonists is perturbed in Akita mice indicating that this is an important mechanism underlying the altered parasympathetic responsiveness of the SAN in the diabetic heart. Changes in electrical conduction and location of the leading pacemaker site in the SAN are influenced by several factors including spontaneous AP firing properties (and the ion channels that underlie this), cell to cell communication and the extent of fibrosis [39,40]. We have demonstrated that Akita hearts display alterations in AP firing

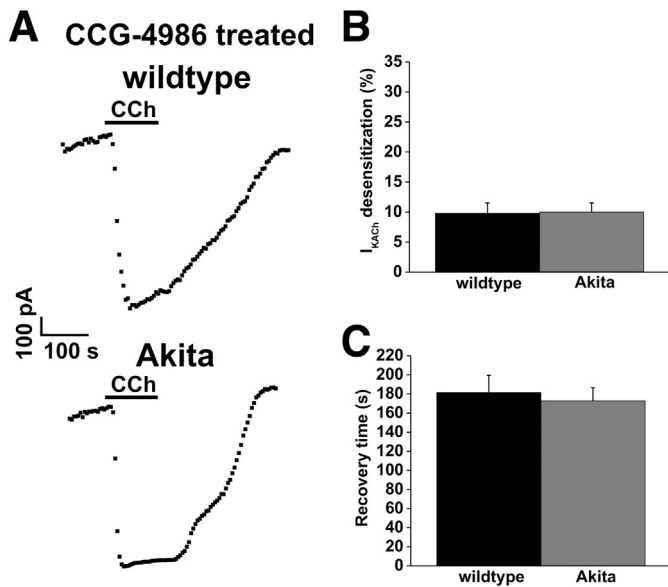


Fig. 8. Kinetic properties of $I_{K_{ACh}}$ in SAN myocytes from Akita mice treated with the RGS4 inhibitor CCG-4986. CCG-4986 (10 μ M) was included in the recording pipette and dialyzed into SAN myocytes for 5 min before the effects of CCh (10 μ M) were studied. (A) Representative time course recordings illustrating the kinetic properties of $I_{K_{ACh}}$ measured at -100 mV in wildtype and Akita SAN myocytes treated with CCG-4986. Scale bars are identical for both recordings. (B) Summary data illustrating the extent of $I_{K_{ACh}}$ desensitization in wildtype and Akita SAN myocytes treated with CCG-4986. (C) Summary data illustrating the time course of recovery of $I_{K_{ACh}}$ to baseline in wildtype and Akita SAN myocytes treated with CCG-4986. There were no differences in $I_{K_{ACh}}$ desensitization ($P = 0.928$) or recovery time ($P = 0.712$) between wildtype and Akita SAN myocytes following CCG-4986 treatment. Data analyzed by Student's t -test; $n = 8$ wildtype and 9 Akita SAN myocytes.

and $I_{K_{ACh}}$ properties as well as increases in extracellular matrix deposition. Based on these findings, it is possible that enhanced fibrosis is disrupting cell to cell communication and contributing to the alterations in SAN conduction during parasympathetic signaling along with the alterations in $I_{K_{ACh}}$ in SAN myocytes. Consistent with this possibility, we demonstrated that insulin treatment effectively normalized HR and SAN function (*in vivo*) and potentially prevented the development of atrial fibrosis. We did not perform optical mapping studies in insulin treated hearts; however, based on the ability of insulin to correct SAN function *in vivo* and prevent fibrosis; it is likely that insulin treatment would also reverse the alterations in electrical conduction in the SAN in Akita mice.

The observation that the effects of CCh on AP firing in Akita and wildtype SAN myocytes correlated with changes in MDP as well as DD slope prompted us to investigate the roles of $I_{K_{ACh}}$ and I_f in the diabetic heart. Our experiments demonstrate that, in terms of parasympathetic responsiveness, only $I_{K_{ACh}}$ was altered in Akita SAN myocytes, suggesting that $I_{K_{ACh}}$ is the critical ionic current involved in this response. Although CCh reduced the DD slope to a smaller extent in Akita SAN myocytes there was no difference in the reduction of I_f by CCh in these cells. This suggests that the reduced effects of CCh on DD slope are associated with alterations in $I_{K_{ACh}}$ and the magnitude of membrane hyperpolarization.

$I_{Ca,L}$ is also known to be modulated by parasympathetic agonists; however, a number of studies have shown that muscarinic regulation of $I_{Ca,L}$ is dependent on previous β -adrenergic receptor stimulation [4, 5]. Thus, $I_{Ca,L}$ is unlikely to contribute to impaired parasympathetic regulation of the SAN in Akita mice in our experimental conditions (*i.e.* where we have not used β -agonists). Consistent with this hypothesis, we observed no effects of CCh on the AP take off potential in SAN myocytes from wildtype or Akita mice, which would be expected if $I_{Ca,L}$ was being modulated. Nevertheless, $I_{Ca,L}$ (or other currents such as I_f) could contribute to altered parasympathetic regulation in the

diabetic heart in the setting of simultaneous or prior activation of the sympathetic nervous system.

Since the main alterations in $I_{K_{ACh}}$ in Akita SAN myocytes were related to the desensitization and deactivation kinetics of the current we focused on the role of RGS4 in the diabetic heart. RGS4 is a GTPase activating protein that enhances the termination of $G_{i/o}$ signaling by promoting the exchange of GTP for GDP on the α subunit of $G_{i/o}$ proteins [41,42]. RGS proteins have been directly implicated in parasympathetic regulation of HR [43,44]. RGS4, in particular, regulates $I_{K_{ACh}}$ downstream of M_2 receptors [45,46] and we recently demonstrated that RGS4 is a critical regulator of parasympathetic responses in SAN myocytes through effects on $I_{K_{ACh}}$ [31,47]. In particular, we showed that RGS4 knockout mice are characterized by enhanced parasympathetic signaling in the SAN due to a reduction in $I_{K_{ACh}}$ desensitization and a slowing of $I_{K_{ACh}}$ deactivation kinetics (*i.e.* opposite responses to those seen in Akita mice) without changes in peak $I_{K_{ACh}}$.

The observation that $I_{K_{ACh}}$ in Akita SAN myocytes was also characterized by altered desensitization and deactivation kinetics without changes in peak current strongly implicates RGS4 and suggests the possibility of enhanced RGS4 activity in the Akita SAN. We utilized a selective RGS4 antagonist, CCG-4986 [35,36], and found that it decreased $I_{K_{ACh}}$ desensitization and prolonged $I_{K_{ACh}}$ recovery in wildtype and Akita SAN myocytes to values very comparable to those we measured in RGS knockout mice [31]. The effects of CCG-4986 were larger in Akita SAN myocytes compared to wildtype SAN myocytes so that the differences in $I_{K_{ACh}}$ properties between wildtype and Akita mice were abolished. Importantly, RGS4 is known to be inhibited by PIP_3 [33,34] providing a direct link between our studies with PIP_3 treatment and RGS4 inhibition in Akita mice. These data strongly suggest that RGS4 activity is enhanced in the SAN of diabetic mice due to the loss of insulin-dependent activation of PI3K (p110 α isoform) [32] and PIP_3 . Impaired PI3K/ PIP_3 signaling is known to contribute to the progression of diabetic complications in the heart [48,49]. Future studies could use the RGS4 knockout mouse to further study the role of this protein in the diabetic heart.

It is important to note that insulin signaling, including *via* PI3K, is highly complex and involves a large number of signaling pathways [49]. Indeed, recent studies have shown that $I_{K_{ACh}}$ is modulated in atrial (but not SAN) myocytes from Akita mice *via* sterol regulatory element binding proteins and glycogen synthase kinase- β [21,50], the latter of which is also activated downstream of PI3K. Additional studies will be needed to determine whether any of these additional mechanisms and/or signaling pathways contribute to the altered parasympathetic responsiveness within SAN myocytes in the diabetic heart.

While the main focus of our study was on parasympathetic regulation of the SAN in diabetes our experiments also clearly show that there are baseline reductions in HR and SAN function in Akita mice. This is consistent with a prior study [25] that also showed baseline reductions in SAN function, which were due to fibrosis in the SAN and apoptosis of SAN myocytes. Consistently, our study also shows that baseline differences in SAN function in Akita mice are associated with structural remodeling (*i.e.* fibrosis) of the atria rather than differences in basal spontaneous AP morphology. Together, this prior work and our present study demonstrate that an important component of cardiovascular complications of diabetes involve the SAN and suggest that altered SAN physiology contributes to death and morbidity in diabetic patients.

In summary, we have identified a novel mechanism for the impaired regulation of HR by the parasympathetic nervous system in the diabetic heart. This involves a reduction in responsiveness of the SAN to parasympathetic agonists in association with blunted effects of CCh on electrical conduction in the SAN and spontaneous AP firing in SAN myocytes. Our mechanistic studies demonstrate that $I_{K_{ACh}}$ plays a key role in these alterations and that $I_{K_{ACh}}$ is altered due to a loss of insulin dependent PI3K/ PIP_3 signaling and the subsequent regulation of RGS4 activity. This work identifies new potential targets for intervention in diabetic patients.

Funding

This work was supported by operating grants from the Nova Scotia Health Research Foundation, The Canadian Institutes of Health Research (CIHR; MOP 93718) and the Heart and Stroke Foundation of Canada to RAR who holds New Investigator Awards from The Heart and Stroke Foundation of Canada and the CIHR. EEE is the recipient of a Heart and Stroke Foundation Fellowship award.

Disclosures

None.

Appendix A. Supplementary data

Supplementary data to this article can be found online at <http://dx.doi.org/10.1016/j.yjmcc.2015.02.024>.

References

- Vinik AI, Ziegler D. Diabetic cardiovascular autonomic neuropathy. *Circulation* 2007; 115:387–97.
- Weston PJ, Gill GV. Is undetected autonomic dysfunction responsible for sudden death in Type 1 diabetes mellitus? The 'dead in bed' syndrome revisited. *Diabet Med* 1999;16:626–31.
- Maser RE, Mitchell BD, Vinik AI, Freeman R. The association between cardiovascular autonomic neuropathy and mortality in individuals with diabetes: a meta-analysis. *Diabetes Care* 2003;26:1895–901.
- Mangoni ME, Nargeot J. Genesis and regulation of the heart automaticity. *Physiol Rev* 2008;88:919–82.
- Irisawa H, Brown HF, Giles W. Cardiac pacemaking in the sinoatrial node. *Physiol Rev* 1993;73:197–227.
- DiFrancesco D. Pacemaker mechanisms in cardiac tissue. *Annu Rev Physiol* 1993;55: 455–72.
- Lakatta EG, Maltsev VA, Vinogradova TM. A coupled SYSTEM of intracellular Ca²⁺ clocks and surface membrane voltage clocks controls the timekeeping mechanism of the heart's pacemaker. *Circ Res* 2010;106:659–73.
- Gehrmann J, Meister M, Maguire CT, Martins DC, Hammer PE, Neer EJ, et al. Impaired parasympathetic heart rate control in mice with a reduction of functional G protein betagamma-subunits. *Am J Physiol Heart Circ Physiol* 2002;282:H445–56.
- Wickman K, Nemej J, Gendler SJ, Clapham DE. Abnormal heart rate regulation in GIRK4 knockout mice. *Neuron* 1998;20:103–14.
- Mesirca P, Marger L, Toyoda F, Rizzetto R, Audoubert M, Dubel S, et al. The G-protein-gated K⁺ channel, IKACH, is required for regulation of pacemaker activity and recovery of resting heart rate after sympathetic stimulation. *J Gen Physiol* 2013; 142:113–26.
- Choate JK, Feldman R. Neuronal control of heart rate in isolated mouse atria. *Am J Physiol Heart Circ Physiol* 2003;285:H1340–6.
- Yoshioka M, Kayo T, Ikeda T, Koizumi A. A novel locus, Mody4, distal to D7Mit189 on chromosome 7 determines early-onset NIDDM in nonobese C57BL/6 (Akita) mutant mice. *Diabetes* 1997;46:887–94.
- Kayo T, Koizumi A. Mapping of murine diabetogenic gene mody on chromosome 7 at D7Mit258 and its involvement in pancreatic islet and beta cell development during the perinatal period. *J Clin Invest* 1998;101:2112–8.
- Hsueh W, Abel ED, Breslow JL, Maeda N, Davis RC, Fisher EA, et al. Recipes for creating animal models of diabetic cardiovascular disease. *Circ Res* 2007;100: 1415–27.
- Egom EE, Vella K, Hua R, Jansen HJ, Moghtadaei M, Polina I, et al. Impaired sinoatrial node function and increased susceptibility to atrial fibrillation in mice lacking natriuretic peptide receptor C. *J Physiol* 2015;593:1127–46.
- Azer J, Hua R, Krishnaswamy PS, Rose RA. Effects of natriuretic peptides on electrical conduction in the sinoatrial node and atrial myocardium of the heart. *J Physiol* 2014; 592:1025–45.
- Springer J, Azer J, Hua R, Robbins C, Adamczyk A, McBoyle S, et al. The natriuretic peptides BNP and CNP increase heart rate and electrical conduction by stimulating ionic currents in the sinoatrial node and atrial myocardium following activation of guanylyl cyclase-linked natriuretic peptide receptors. *J Mol Cell Cardiol* 2012;52: 1122–34.
- Azer J, Hua R, Vella K, Rose RA. Natriuretic peptides regulate heart rate and sinoatrial node function by activating multiple natriuretic peptide receptors. *J Mol Cell Cardiol* 2012;53:715–24.
- Hua R, Adamczyk A, Robbins C, Ray G, Rose RA. Distinct patterns of constitutive phosphodiesterase activity in mouse sinoatrial node and atrial myocardium. *PLoS One* 2012;7:e47652.
- Bugger H, Boudina S, Hu XX, Tuinei J, Zaha VG, Theobald HA, et al. Type 1 diabetic Akita mouse hearts are insulin sensitive but manifest structurally abnormal mitochondria that remain coupled despite increased uncoupling protein 3. *Diabetes* 2008;57:2924–32.
- Park HJ, Zhang Y, Du C, Welzig CM, Madias C, Aronovitz MJ, et al. Role of SREBP-1 in the development of parasympathetic dysfunction in the hearts of type 1 diabetic Akita mice. *Circ Res* 2009;105:287–94.
- Basu R, Oudit GY, Wang X, Zhang L, Ussher JR, Lopaschuk GD, et al. Type 1 diabetic cardiomyopathy in the Akita (Ins2WT/C96Y) mouse model is characterized by lipotoxicity and diastolic dysfunction with preserved systolic function. *Am J Physiol Heart Circ Physiol* 2009;297:H2096–108.
- Narula OS, Samet P, Javier RP. Significance of the sinus-node recovery time. *Circulation* 1972;45:140–58.
- Chadda KD, Banka VS, Bodenheimer MM, Helfant RH. Corrected sinus node recovery time. Experimental physiologic and pathologic determinants. *Circulation* 1975;51: 797–801.
- Luo M, Guan X, Luczak ED, Lang D, Kutschke W, Gao Z, et al. Diabetes increases mortality after myocardial infarction by oxidizing CaMKII. *J Clin Invest* 2013;123: 1262–74.
- Fedorov VV, Hucker WJ, Dobrzynski H, Rosenshtraukh LV, Efimov IR. Postganglionic nerve stimulation induces temporal inhibition of excitability in rabbit sinoatrial node. *Am J Physiol Heart Circ Physiol* 2006;291:H612–23.
- Glukhov AV, Fedorov VV, Anderson ME, Mohler PJ, Efimov IR. Functional anatomy of the murine sinus node: high-resolution optical mapping of ankyrin-B heterozygous mice. *Am J Physiol Heart Circ Physiol* 2010;299:H482–91.
- Bleeker WK, Mackaay AJ, Masson-Pevet M, Bouman LN, Becker AE. Functional and morphological organization of the rabbit sinus node. *Circ Res* 1980;46:11–22.
- Verheijck EE, van Kempen MJ, Veereschild M, Lurvink J, Jongasma HJ, Bouman LN. Electrophysiological features of the mouse sinoatrial node in relation to connexin distribution. *Cardiovasc Res* 2001;52:40–50.
- Lomax AE, Rose RA, Giles WR. Electrophysiological evidence for a gradient of G protein-gated K⁺ current in adult mouse atria. *Br J Pharmacol* 2003;140:576–84.
- Cifelli C, Rose RA, Zhang H, Voigtlaender-Bolz J, Bolz SS, Backx PH, et al. RGS4 regulates parasympathetic signaling and heart rate control in the sinoatrial node. *Circ Res* 2008;103:527–35.
- Oudit GY, Sun H, Kerfant BG, Crackower MA, Penninger JM, Backx PH. The role of phosphoinositide-3 kinase and PTEN in cardiovascular physiology and disease. *J Mol Cell Cardiol* 2004;37:449–71.
- Ishii M, Inanobe A, Kurachi Y. PIP3 inhibition of RGS protein and its reversal by Ca²⁺/calmodulin mediate voltage-dependent control of the G protein cycle in a cardiac K⁺ channel. *Proc Natl Acad Sci U S A* 2002;99:4325–30.
- Popov SG, Krishna UM, Falck JR, Wilkie TM. Ca²⁺/Calmodulin reverses phosphatidylinositol 3,4,5-trisphosphate-dependent inhibition of regulators of G protein-signaling GTPase-activating protein activity. *J Biol Chem* 2000;275:18962–8.
- Roman DL, Talbot JN, Roof RA, Sunahara RK, Traynor JR, Neubig RR. Identification of small-molecule inhibitors of RGS4 using a high-throughput flow cytometry protein interaction assay. *Mol Pharmacol* 2007;71:169–75.
- Roman DL, Blazer LL, Monroy CA, Neubig RR. Allosteric inhibition of the regulator of G protein signaling-Galpha protein-protein interaction by CCG-4986. *Mol Pharmacol* 2010;78:360–5.
- Thackeray JT, Beanlands RS, Dasilva JN. Altered sympathetic nervous system signaling in the diabetic heart: emerging targets for molecular imaging. *Am J Nucl Med Mol Imaging* 2012;2:314–34.
- Vinogradova TM, Fedorov VV, Yuzyuk TN, Zaitsev AV, Rosenshtraukh LV. Local cholinergic suppression of pacemaker activity in the rabbit sinoatrial node. *J Cardiovasc Pharmacol* 1998;32:413–24.
- Fedorov VV, Glukhov AV, Chang R. Conduction barriers and pathways of the sinoatrial pacemaker complex: their role in normal rhythm and atrial arrhythmias. *Am J Physiol Heart Circ Physiol* 2012;302:H1773–83.
- Wolf RM, Glynn P, Hashemi S, Zarei K, Mitchell CC, Anderson ME, et al. Atrial fibrillation and sinus node dysfunction in human ankyrin-B syndrome: a computational analysis. *Am J Physiol Heart Circ Physiol* 2013;304:H1253–66.
- Watson N, Linder ME, Druey KM, Kehrl JH, Blumer KJ. RGS family members: GTPase-activating proteins for heterotrimeric G-protein alpha-subunits. *Nature* 1996;383: 172–5.
- Wieland T, Mittmann C. Regulators of G-protein signalling: multifunctional proteins with impact on signalling in the cardiovascular system. *Pharmacol Ther* 2003;97: 95–115.
- Fu Y, Huang X, Zhong H, Mortensen RM, D'Alecy LG, Neubig RR. Endogenous RGS proteins and Galpha subtypes differentially control muscarinic and adenosine-mediated chronotropic effects. *Circ Res* 2006;98:659–66.
- Fu Y, Huang X, Piao L, Lopatin AN, Neubig RR. Endogenous RGS proteins modulate SA and AV nodal functions in isolated heart: implications for sick sinus syndrome and AV block. *Am J Physiol Heart Circ Physiol* 2007;292:H2532–9.
- Doupnik CA, Davidson N, Lester HA, Kofuji P. RGS proteins reconstitute the rapid gating kinetics of gbetagamma-activated inwardly rectifying K⁺ channels. *Proc Natl Acad Sci U S A* 1997;94:10461–6.
- Zhang Q, Pacheco MA, Doupnik CA. Gating properties of GIRK channels activated by Galpha(i)- and Galpha(i)-coupled muscarinic m2 receptors in *Xenopus* oocytes: the role of receptor precoupling in RGS modulation. *J Physiol* 2002;545:355–73.
- Neubig RR. And the winner is ... RGS4! *Circ Res* 2008;103:444–6.
- Lu Z, Jiang YP, Xu XH, Ballou LM, Cohen IS, Lin RZ. Decreased L-type Ca²⁺ current in cardiac myocytes of type 1 diabetic Akita mice due to reduced phosphatidylinositol 3-kinase signaling. *Diabetes* 2007;56:2780–9.
- Abel ED. Insulin signaling in heart muscle: lessons from genetically engineered mouse models. *Curr Hypertens Rep* 2004;6:416–23.
- Zhang Y, Welzig CM, Picard KL, Du C, Wang B, Pan JQ, et al. Glycogen synthase kinase-3beta inhibition ameliorates cardiac parasympathetic dysfunction in type 1 diabetic Akita mice. *Diabetes* 2014;63:2097–113.

Altered parasympathetic nervous system regulation of the sinoatrial node in Akita diabetic mice

Online Supplement

Methods

Animals

This study utilized male littermate wildtype and type 1 diabetic Akita mice between the ages of 16 and 20 weeks. Akita mice [1-3] were initially obtained from the Jackson Laboratory (strain C57BL/6-*Ins2*^{Akita}/J) and then bred locally in the Carleton Animal Facility at Dalhousie University. This mouse contains a mutation in the insulin-2 (*Ins2*) gene, *Ins2*^{C96Y}, which results in severe pancreatic β cell dysfunction and development of the diabetic phenotype [4]. Heterozygous Akita mice (diabetic) and littermate wildtypes were used in this study. Progression of diabetes and genotyping was determined by assessing urine glucose, protein and ketones (using keto-diastring reagent strips for urinalysis) as well as serum glucose levels (using a glucometer).

In some experiments Akita mice were treated with insulin (or placebo) for 4 weeks beginning at 12 weeks of age. This was done by implanting insulin pellets (or placebo) (LinShin Canada) subcutaneously. These pellets release 0.2 units of insulin/day. Mice were anesthetized by isoflurane inhalation (3%) and pellets were implanted via a small puncture in the skin according to the manufacturer's instructions. Blood glucose was monitored in these animals before pellet implantation and then every 3 days after treatment began until the animals were used experimentally at 16 weeks of age (similar to all other experimental groups).

All experimental procedures were approved by the Dalhousie University Committee for Laboratory Animals and conformed to the guidelines of the Canadian Council on Animal Care.

***In vivo* electrophysiology, programmed stimulation and Langendorff preparation**

Surface ECGs (used to assess changes in heart rate) were measured in anesthetized mice (2% isoflurane inhalation) using 30 gauge subdermal needle electrodes (Grass Technologies). A 1.2 french octapolar electrophysiology catheter containing 8 electrodes spaced 0.5 mm apart (Transonic) was used for intracardiac pacing experiments. Correct catheter placement was ensured by obtaining a sole ventricular signal in the distal lead and a predominant atrial signal in the proximal lead. All stimulation pulses were given at 0.4 mA for 2 ms, which enabled continuous capture and drive of cardiac conduction. Sinoatrial node recovery time (SNRT) was measured by delivering a 12 stimulus drive train at a cycle length of 100 ms. SNRT is defined as the time between the last stimulus in the drive train and the occurrence of the first spontaneous atrial beat (P wave). SNRT was corrected for heart rate (cSNRT) by subtracting the prestimulus RR interval from the measured SNRT. Data were acquired using a Gould ACQ-7700 amplifier and Ponemah Physiology Platform software (Data Sciences International) as we have described previously [5]. Body temperature was monitored continuously via a rectal probe and maintained at 37°C with a heating pad.

We also recorded surface ECGs in isolated Langendorff-perfused hearts as we have done previously [6, 7]. In these studies, hearts were retrogradely perfused via the aorta with a normal Tyrode's solution consisting of (in mM) 140 NaCl, 5.4 KCl, 1.2 KH₂PO₄,

1.0 MgCl₂, 1.8 CaCl₂, 5.55 glucose, and 5 HEPES, with pH adjusted to 7.4 with NaOH. Hearts were perfused at a fixed rate of 2.5 mL/min and temperature was maintained at 37°C. We did not observe any differential changes in flow rate after application of CCh between wildtype and Akita mice.

High resolution optical mapping

To study patterns of electrical conduction in the sinoatrial node (SAN) we used high resolution optical mapping in atrial preparations (Supplemental Fig. 4) as we have done previously [8]. To isolate our atrial preparation mice were administered a 0.2 ml intraperitoneal injection of heparin (1000 IU/ml) to prevent blood clotting and were then anesthetized by isoflurane inhalation and cervically dislocated. Hearts were excised into Krebs solution (35°C) containing (in mM): 118 NaCl, 4.7 KCl, 1.2 KH₂PO₄, 12.2 MgSO₄, 1 CaCl₂, 25 NaHCO₃, 11 glucose and bubbled with 95% O₂/5% CO₂ in order to maintain a pH of 7.4. The atria were dissected away from the ventricles and pinned in a dish with the endocardial surface facing upwards (towards the imaging equipment). The superior and inferior vena cavae were cut open so that the crista terminalis could be visualized. The SAN area is located in the intercaval region in the right atrial posterior wall adjacent to the crista terminalis [6-11].

The atrial preparation was superfused continuously with Krebs solution (37°C) bubbled with 95% O₂/5% CO₂ and allowed to equilibrate for at least 30 min. During this time the preparation was treated with the voltage sensitive dye di-4-ANEPPS (10 μM) and blebbistatin (10 μM) was added to the superfusate to suppress contractile activity [12, 13]. Blebbistatin was present throughout the duration of the experiments in order prevent motion artifacts during

optical mapping. Some experiments were performed in sinus rhythm so that the cycle length (i.e. beating rate) of the atrial preparation was free to change. In some studies we used a pacing electrode to pace atrial preparations at a fixed cycle length of 120 ms in order to study electrical conduction independently of changes in cycle length. The pacing electrode was placed near the opening of the superior vena cava.

Di-4-ANEPPS loaded atrial preparations were illuminated with light at a wavelength of 520 – 570 nm using an EXFO X-cite fluorescent light source (Lumen Dynamics). Emitted fluorescent light (590 – 640 nm) was captured using a high speed EMCCD camera (Evolve 128, Photometrics). We mapped conduction in the region of the right atrial posterior wall around the point of initial electrical excitation (Supplemental Fig. 4), which corresponds to the activation of the SAN [8, 14, 15]. The region that was mapped extended from the superior vena cava to the inferior cava along the edge of the CT, based on the known anatomical location of the SAN in the mouse heart [11]. In these studies the spatial resolution of each pixel was 45 x 45 μM and data were acquired at 600 frames/s using Metamorph software (Molecular Devices). Magnification was constant in all experiments and no pixel binning was used.

The location of the leading pacemaker site was assessed in baseline conditions and following application of CCh. Shifts in leading pacemaker site were quantified using a grid (see Figure 4 in manuscript) in which the vertical axis was placed parallel, and just adjacent to the crista terminalis. The horizontal axis was placed along the edge of the opening of the inferior vena cava, perpendicular to the vertical axis. Straight lines were drawn between the leading pacemaker sites in baseline conditions and after application of CCh in wildtype and Akita atrial preparations.

All optical data were analyzed using custom software written in Matlab. Analyses included pseudocolor electrical activation maps, which were generated from measurements of activation time at individual pixels. In all cases background fluorescence was subtracted. Local conduction velocity (CV) was quantified specifically in the SAN around the site of initial electrical activation in the right atrial posterior wall using an established approach previously described [8, 16, 17]. Briefly, activation times at each pixel from a 7 x 7 pixel array were determined and fit to a plane using the least squares fit method. The direction on this plane that is increasing the fastest represents the direction that is perpendicular to the wavefront of electrical propagation and the maximum slope represents the inverse of the speed of conduction in that direction. Thus, using this method, we computed maximum local CV vectors in the SAN around the leading pacemaker site. With pixel dimensions of 45 x 45 μM , the area of the 7 x 7 pixel array was 315 x 315 μM , which is within the anatomical area of the mouse SAN [11]. In some experiments we also generated optical action potential data by measuring changes in fluorescence as a function of time at individual pixels within the SAN as we have described previously [8].

Isolation of mouse sinoatrial node myocytes

The procedures for isolating single pacemaker myocytes from the SAN in mice have been described previously [6, 18] and were as follows. Mice were administered a 0.2 ml intraperitoneal injection of heparin (1000 IU/ml) to prevent blood clotting. Following this, mice were anesthetized by isoflurane inhalation and then sacrificed by cervical dislocation. The heart was excised into Tyrode's solution (35°C) consisting of (in mM) 140 NaCl, 5.4 KCl, 1.2 KH_2PO_4 , 1.0 MgCl_2 , 1.8 CaCl_2 , 5.55 glucose, and 5 HEPES, with pH adjusted to 7.4 with NaOH.

Atrial preparations (as described above) were dissected and the SAN region was cut into strips, which were transferred and rinsed in a 'low Ca^{2+} , Mg^{2+} free' solution containing (in mM) 140 NaCl, 5.4 KCl, 1.2 KH_2PO_4 , 0.2 CaCl_2 , 50 taurine, 18.5 glucose, 5 HEPES and 1 mg/ml bovine serum albumin (BSA), with pH adjusted to 6.9 with NaOH. SAN tissue strips were digested in 5 ml of 'low Ca^{2+} , Mg^{2+} free' solution containing collagenase (type II, Worthington Biochemical Corporation), elastase (Worthington Biochemical Corporation) and protease (type XIV, Sigma Chemical Company) for 30 min. The tissue was then transferred to 5 ml of modified KB solution containing (in mM) 100 potassium glutamate, 10 potassium aspartate, 25 KCl, 10 KH_2PO_4 , 2 MgSO_4 , 20 taurine, 5 creatine, 0.5 EGTA, 20 glucose, 5 HEPES, and 0.1% BSA, with pH adjusted to 7.2 with KOH. The tissue was mechanically agitated using a wide-bore pipette. This procedure yielded individual SAN myocytes with cellular automaticity that was recovered after readapting the cells to a physiological concentration of Ca^{2+} . SAN myocytes were identified by their small spindle shape and ability to beat spontaneously in the recording chamber when superfused with normal Tyrode's solution. When patch-clamped, SAN myocytes always displayed spontaneous action potentials. The capacitance of single SAN myocytes was 20 – 35 pF.

Solutions and electrophysiological protocols

Spontaneous action potentials were recorded using the perforated patch-clamp technique [19] on single SAN myocytes [6, 7, 18]. The acetylcholine activated K^+ current (I_{KACH}) and the hyperpolarization activated current (I_f) were recorded by voltage clamping single SAN myocytes using the patch-clamp technique in the whole cell configuration [20, 21]. Action potentials and ionic currents were recorded at room temperature (22-23°C), which must be noted when

comparing these data to *in vivo* heart rate measurements. I_{KACH} was investigated using a voltage ramp from +50 mV to -120 mV (holding potential was -80 mV) before and after application of carbachol (CCh; 10 μ M) as we have described previously [21]. I_{KACH} was quantified as the CCh-sensitive difference current. I_f was recorded by applying a series of 2.5 s voltage clamp steps between -150 mV and -30 mV from a holding potential of -35 mV.

For recording APs, I_{KACH} and I_f , the recording chamber was superfused with a normal Tyrode's solution (22 – 23°C) containing (in mM) 140 NaCl, 5 KCl, 1 MgCl₂, 1 CaCl₂, 10 HEPES, and 5 glucose, with pH adjusted to 7.4 with NaOH. The pipette filling solution for I_{KACH} contained (in mM) 135 KCl, 0.1 CaCl₂, 1 MgCl₂, 5 NaCl, 10 EGTA, 4 Mg-ATP, 6.6 Na-phosphocreatine, 0.3 Na-GTP and 10 HEPES, with pH adjusted to 7.2 with KOH. Amphotericin B (200 μ g/ml) was added to this pipette solution to record APs with the perforated patch clamp technique. 2 mM BaCl₂ was added to the superfusate when recording I_f in order to block I_{KACH} [22].

Micropipettes were pulled from borosilicate glass (with filament, 1.5 mm OD, 0.75 mm ID, Sutter Instrument Company) using a Flaming/Brown pipette puller (model p-87, Sutter Instrument Company). The resistance of these pipettes was 4 – 8 M Ω when filled with recording solution. Micropipettes were positioned with a micromanipulator (Burleigh PCS-5000 system) mounted on the stage of an inverted microscope (Olympus IX71). Seal resistance was 2 – 15 G Ω . Rupturing the sarcolemma in the patch for voltage clamp experiments resulted in access resistances of 5 – 15 M Ω . Series resistance compensation averaged 80 – 85% using an Axopatch 200B amplifier (Molecular Devices). For perforated patch clamp experiments access resistance was monitored for the development of capacitative transients upon sealing to the cell membrane with Amphotericin B in the pipette. Typically, access resistance became less than 30 M Ω within

5 min of sealing onto the cell, which was sufficient for recording spontaneous APs in current clamp mode. Data were digitized using a Digidata 1440 and pCLAMP 10 software (Molecular Devices) and stored on computer for analysis.

Spontaneous AP parameters, including the maximum diastolic potential (MDP), the slope of the diastolic depolarization (DD slope) and the take-off potential were analyzed as described previously [6, 7, 9]. The DD slope was measured by fitting a straight line to the initial linear portion (~2/3) of this AP component as we and other have previously done [6, 23]. The take-off potential (the membrane potential at which the AP initiates) was measured at the intersection of two straight lines fitted to the DD slope and the AP upstroke [23].

Quantitative PCR

Quantitative gene expression in SAN, as well as right and left atrial samples, was performed as we have described previously [6, 18]. Intron spanning primers were designed for RGS4, collagen I (*coll1a*), and Collagen III (*col3a*), HCN4, ANP, β -actin (*Actb*) and GAPDH and tested using Amplify 3. Following synthesis (Sigma Genosys) primers were reconstituted to 100 nM in nuclease free water and stored at -20°C until experimental use. HCN4 and ANP were used to distinguish SAN from right atrial samples as we have described previously [6, 18].

Specifically, HCN4 expression is high in the SAN compared to the right atrium while ANP expression is high in the right atrium compared to the SAN. Primer sequences were as follows:

Coll1a:

Forward 5'- GCGGACTCTGTTGCTGCTTGC-3'

Reverse 5'- GACCTGCGGGACCCCTTTGT-3'

Amplification product 124 base pairs

Col3a:

Forward 5' - AGATCCGGGTCCTCCTGGCATTC-3'

Reverse 5' - CTGGTCCCGGATAGCCACCCAT-3'

Amplification product 193 base pairs

RGS4:

Forward 5' -GGGCTGAATCGTTGCAAAC-3'

Reverse 5' -ATTCCGACTTCAGGAAAGCTTT-3'

Amplification product 232 base pairs.

B-actin (*Actb*):

Forward 5' -AGCCATGTACGTAGCCAT -3'

Reverse 5' -TCTCAGCTGTGGTGGTGAAG -3'

Amplification product 227 base pairs.

GAPDH:

Forward 5' -GTGCCAGCCTCGTCCCG-3'

Reverse 5' -CCATGTAGTTGAGGTCAATGAAGGG-3'

Amplification product 151 base pairs.

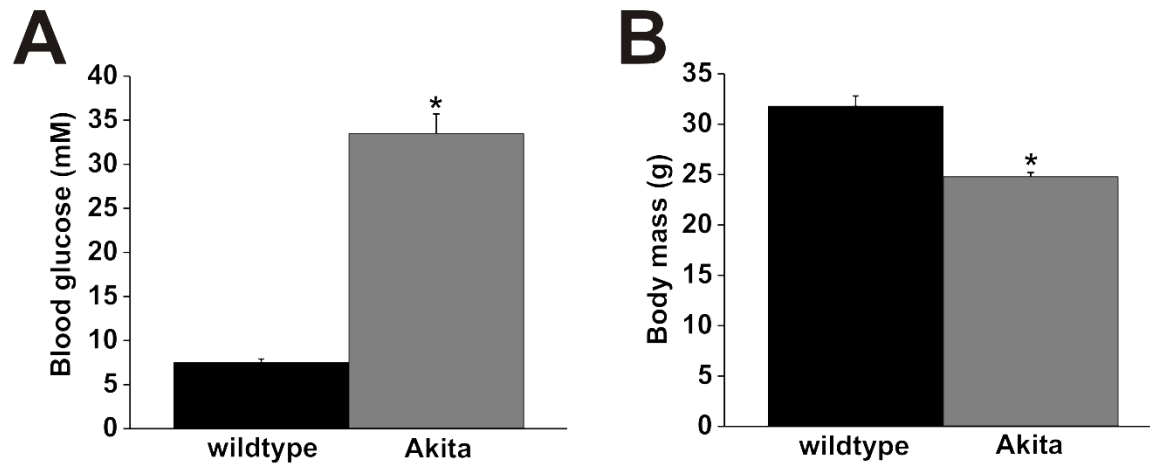
RNA was extracted in PureZOL™ RNA isolation reagent according to kit instructions (Aurum total RNA fatty and fibrous tissue kit, BioRad). Tissue was eluted in 30-40 µl of elution buffer from the spin column. RNA concentrations were determined using a Qubit fluorometer (Invitrogen) and first strand synthesis reactions were performed using the iScript cDNA synthesis kit (BioRad) according to kit directives with 0.5 µg RNA template. A260/280 readings were also performed to evaluate the purity of RNA extractions prior to first strand synthesis. Lack of genomic DNA contamination was verified by reverse transcription (RT)-PCR using a no RT control.

RT-qPCR using BRYT green dye was used to assess gene expression. Following RNA extraction cDNA was synthesized and 20 µl BRYT reactions were performed with 1 µl cDNA template. Reactions were carried out using a CFX96 Real-Time PCR Detection System (BioRad). Amplification conditions were as follows: 95°C for 2 min to activate Taq polymerase, 35 cycles of denaturation at 95°C for 30 sec, annealing using a gradient from 53-61°C for 30 sec and extension at 72°C or 1 min 30 sec. Melt curve analysis was performed from 65-95°C in 0.5°C increments. Single amplicons with appropriate melting temperatures and sizes were detected. C_T values > 32 were eliminated due to lack of reproducibility [24]. Primers were used at a concentration of 10 nM.

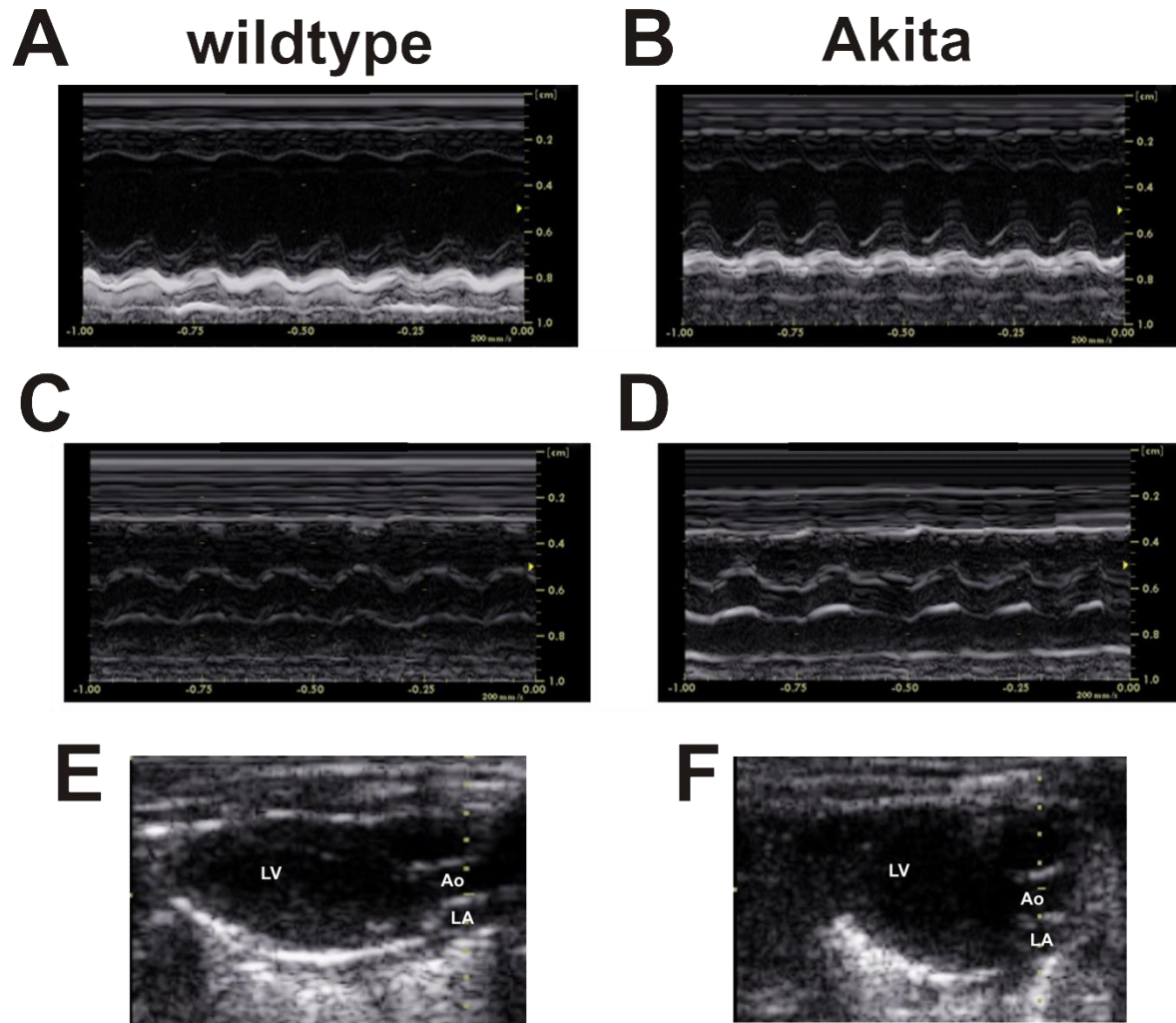
CCh doses

Our study used a number of experimental approaches to investigate parasympathetic regulation of the diabetic heart. For each of these experimental approaches specific CCh doses were chosen. For *in vivo* studies we used a CCh dose of 0.1 mg/kg in order to be comparable to prior studies of CCh effects on the heart, including in diabetic mice [25, 26]. In Langendorff

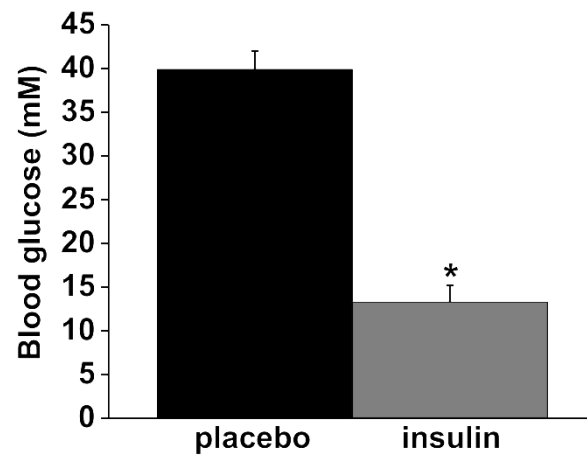
heart studies we used a CCh dose of 1 μM , which elicited robust responses without fully suppressing the heartbeat. For optical mapping studies and spontaneous AP recordings we used a CCh dose of 0.1 μM because higher doses often fully suppressed the preparations. For measurements of I_{KACH} we performed a dose response study with CCh doses from 0.1 – 100 μM . Subsequent pharmacological studies of I_{KACH} as well as studies of I_{f} were performed using a CCh dose of 10 μM in order to elicit maximal responses when studying these currents.

Results

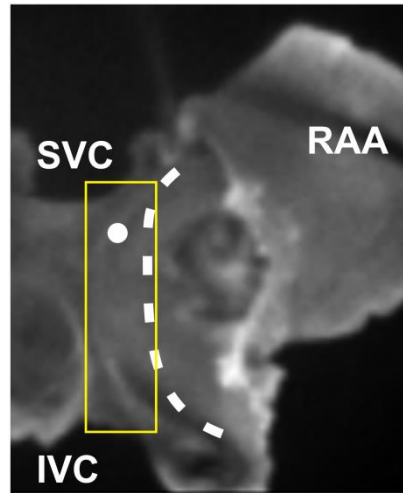
Supplemental Figure 1: Blood glucose and body mass measurements in wildtype and Akita mice. Measurements were taken between the ages of 16-20 weeks. * $P < 0.05$ vs wildtype by Student's t -test; $n = 8$ wildtype and 8 Akita mice.



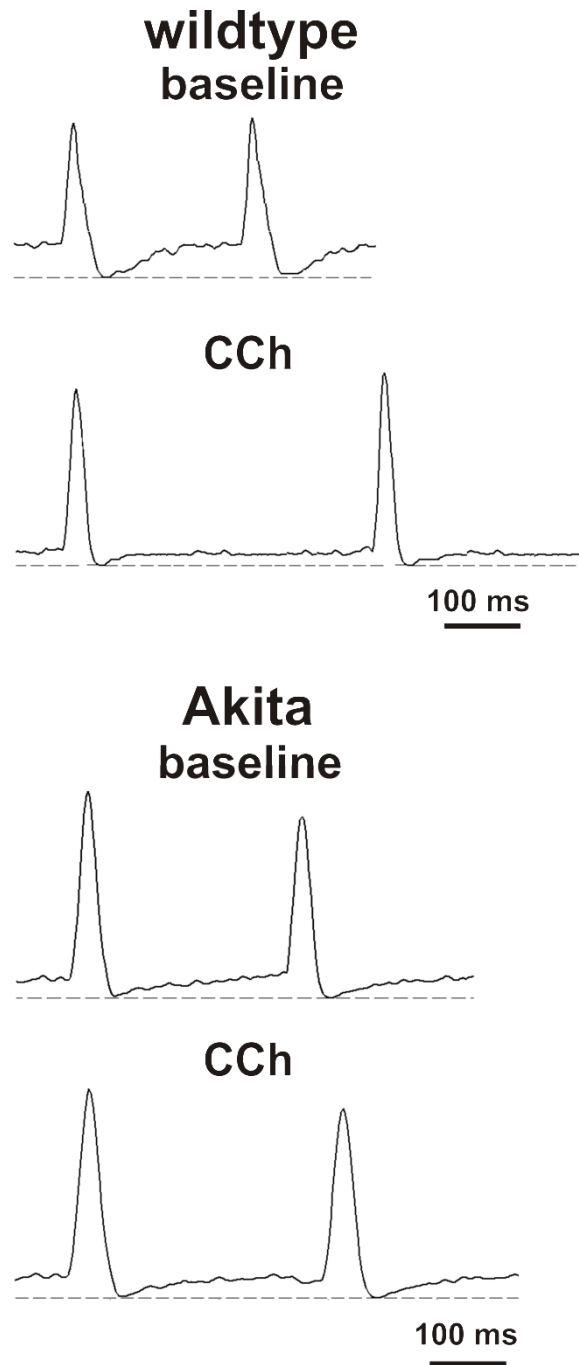
Supplemental Figure 2: Echocardiography of hearts from wildtype and Akita diabetic mice. (A and B) M-mode images from the parasternal short axis view of the heart at the level of the midpapillary muscle in wildtype and Akita mice. (C and D) M-mode images from the parasternal long axis view of the heart in wildtype and Akita mice. (E and F) Representative long axis views of wildtype and Akita hearts. LV, left ventricle; LA, left atrium; Ao, aorta. Dotted lines in E and F indicate the level at which the images in C and D were obtained. Refer to Supplemental Table 1 for a summary of echocardiographic measurements.



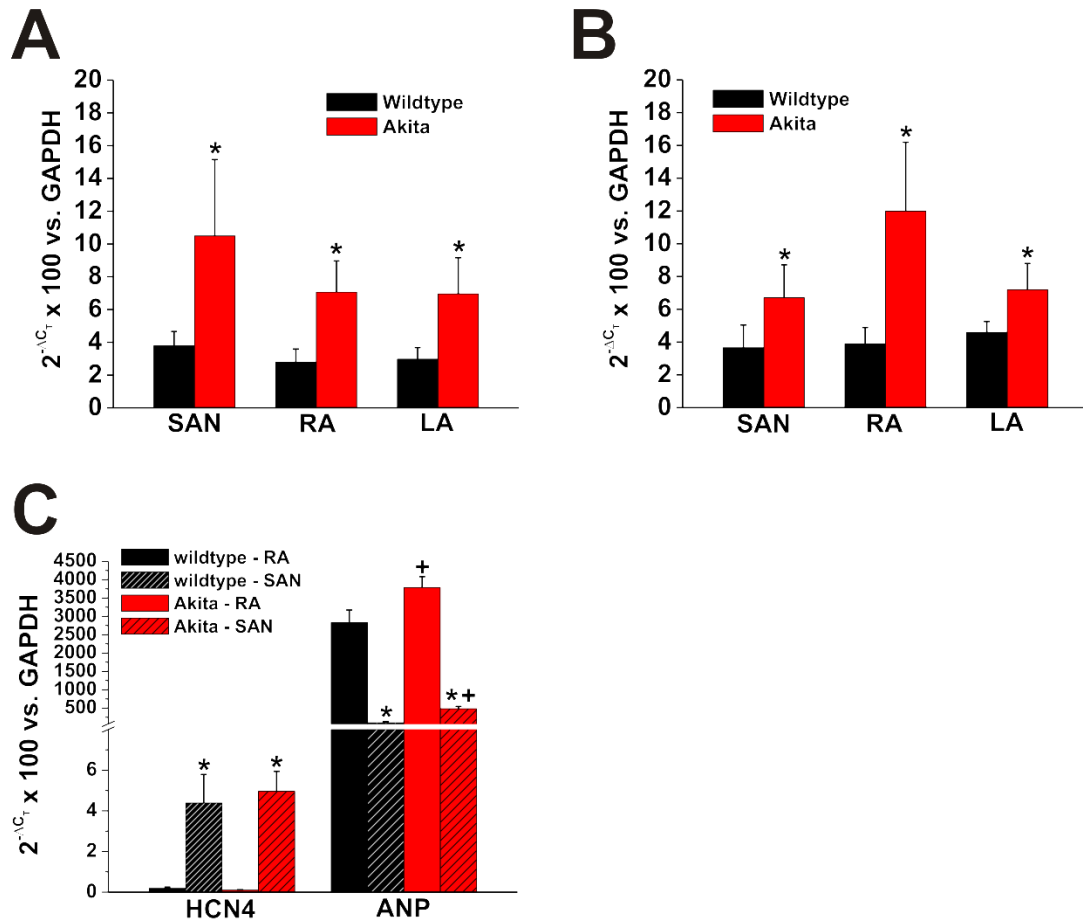
Supplemental Figure 3: Blood glucose measurements in Akita diabetic mice following treatment with insulin. Mice were given insulin pellets or placebo for 4 weeks beginning at 12 weeks of age. * $P < 0.05$ vs. placebo by Student's t -test; $n = 4$ for placebo and 6 for insulin.



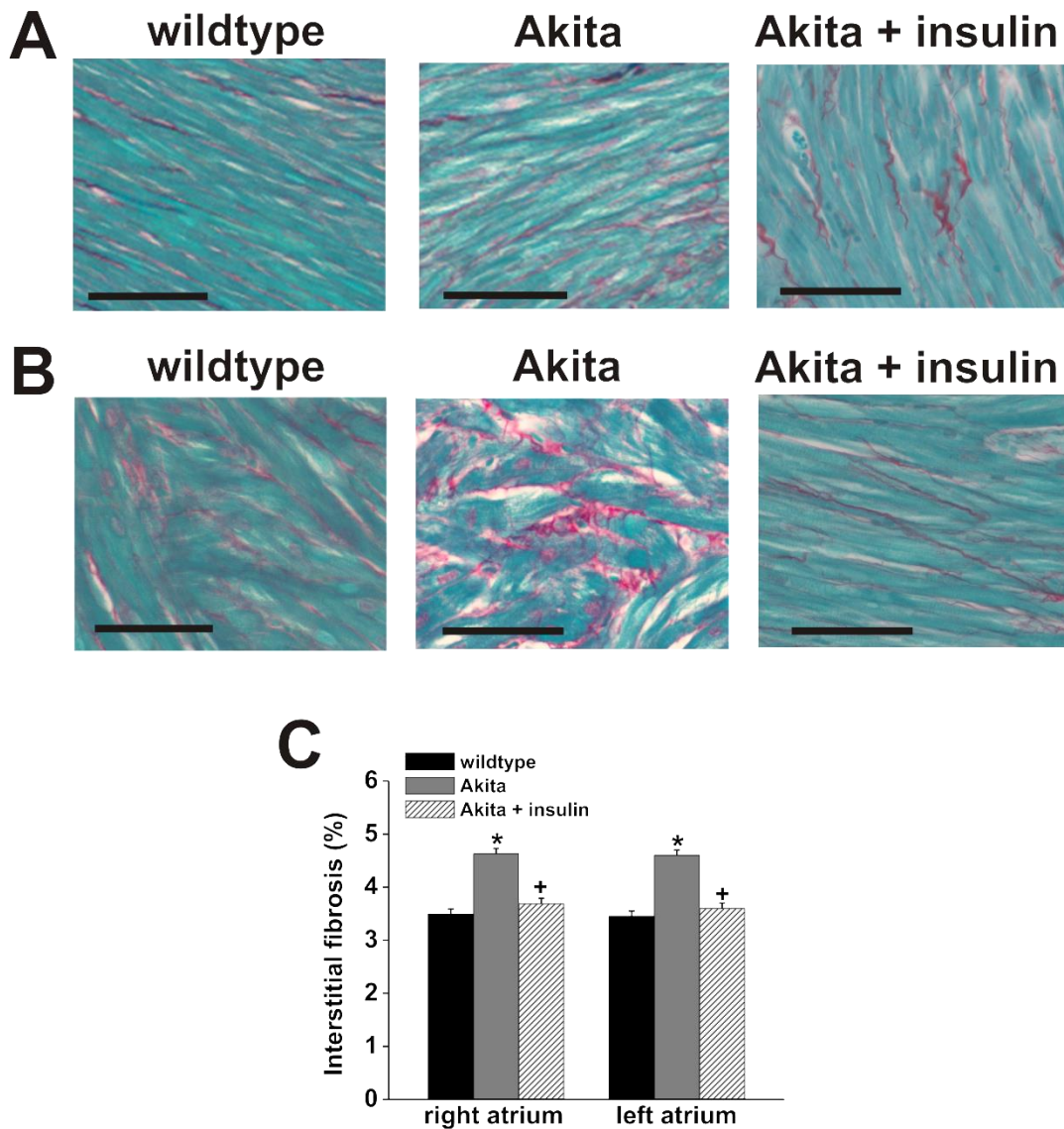
Supplemental Figure 4: Mouse atrial preparation used for optical mapping experiments. The heart is oriented so that the right atrium is on the right side of the image. RAA, right atrial appendage; SVC, opening of the superior vena cava; IVC, opening of the inferior vena cava. The dashed line indicates the location of the crista terminalis (CT). The sinoatrial node is located in the intercaval region adjacent to the CT. The white circle illustrates the typical location of the leading pacemaker site in the SAN within the right atrial posterior wall. The yellow box indicates the typical area that was mapped.



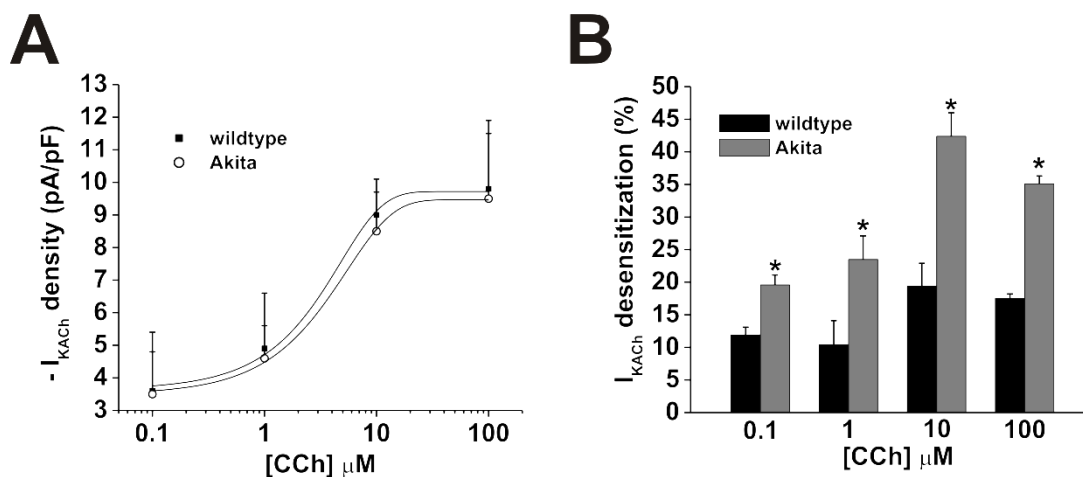
Supplemental Figure 5: Representative optical SAN action potentials from wildtype and Akita hearts. Optical APs were measured in the region of the leading pacemaker site in the right atrial posterior wall in baseline conditions and after application of CCh (0.1 μ M). Dashed horizontal lines are shown through the maximum diastolic potential.



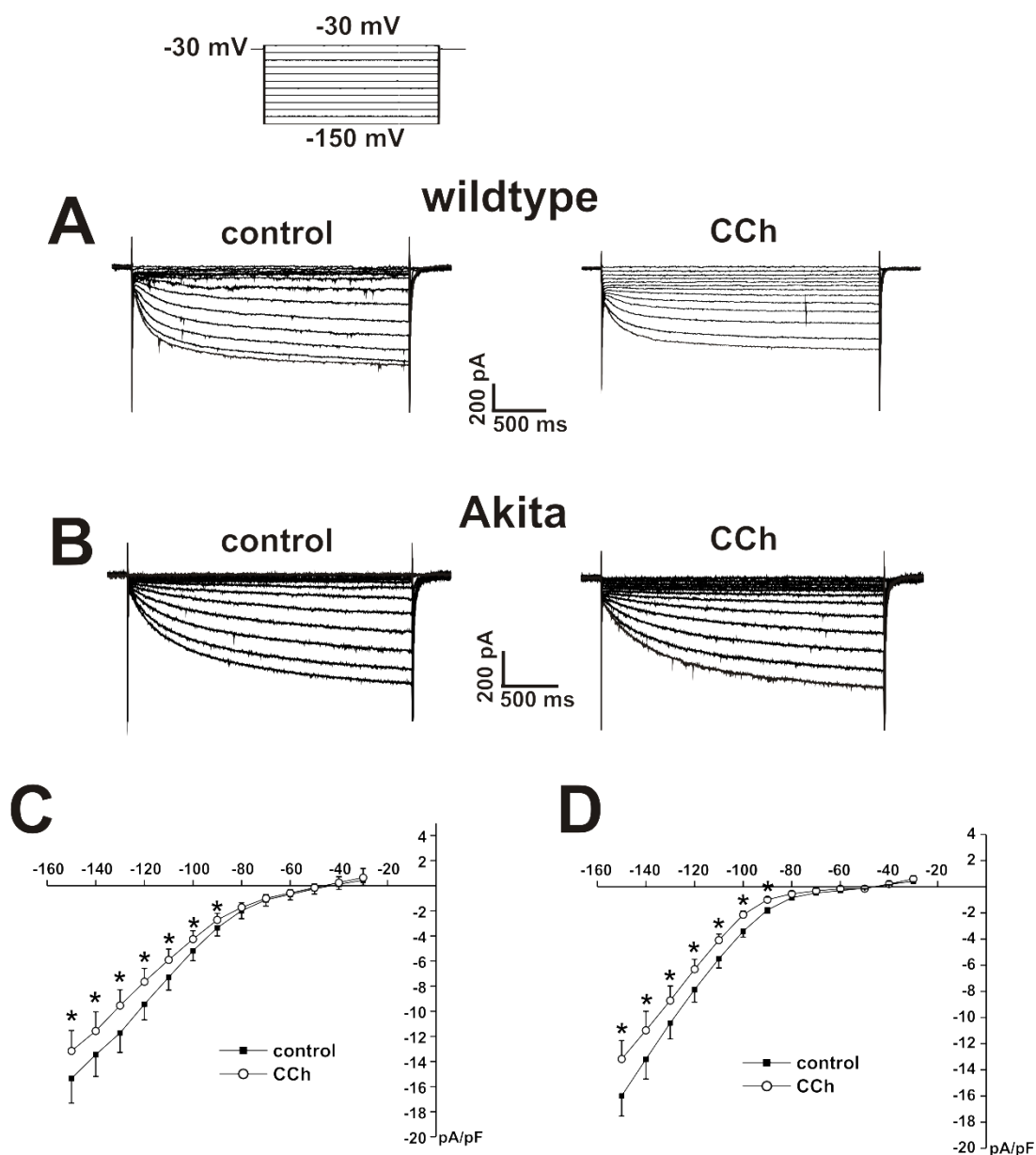
Supplemental Figure 6: Quantitative mRNA expression of collagen I and collagen III in the hearts of wildtype and Akita mice. Expression of collagen I (A) and collagen III (B) was assessed specifically in the SAN, the right atrium (RA) and the left atrium (LA) in wildtype and Akita mice. * $P < 0.05$ vs. wildtype by two-way ANOVA with Tukey's posthoc test. (C) mRNA expression of HCN4 and ANP to confirm that samples used in panels A and B were from the SAN or the right atrium. Note scale break on Y axis. * $P < 0.05$ vs. RA within genotype, ⁺ $P < 0.05$ vs. wildtype within tissue region by two-way ANOVA with Tukey's posthoc test; $n = 8$ hearts for each genotype.



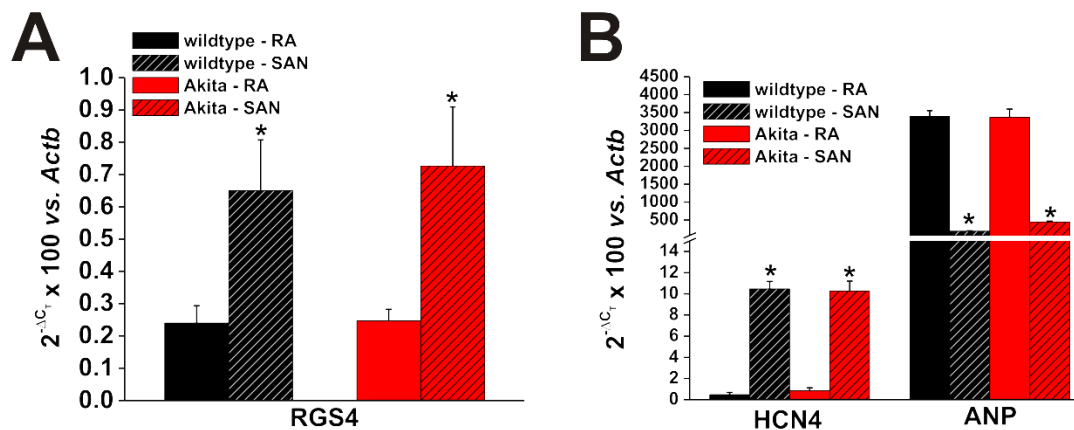
Supplemental Figure 7: Patterns of interstitial fibrosis in the atria of wildtype and Akita mice. Representative images illustrating patterns of collagen deposition (red color) right (**A**) and left (**B**) atria of wildtype mice ($n=4$), Akita mice ($n=4$) and Akita mice treated with insulin ($n=9$). Myocardium is stained green. Scale bars are 50 μ m. (**C**) Quantification of fibrosis from histological sections in the right and left atria * $P<0.05$ vs. wildtype by two-way ANOVA with Tukey's posthoc test.



Supplemental Figure 8: Dose response for the effects of CCh on I_{KACH} in wildtype and Akita SAN myocytes. (A) Dose response curve for the effects of CCh on peak I_{KACH} current density measured at -120 mV before desensitization has occurred. EC_{50} values were $4.31 \pm 1.8 \mu$ M for wildtype and 4.73 ± 1.4 for Akita. There was no difference in peak I_{KACH} density between genotypes at any CCh dose. (B) I_{KACH} desensitization in wildtype and Akita SAN myocytes as a function of CCh dose. * $P < 0.05$ vs wildtype by one-way ANOVA with Tukey's posthoc test. N values for each dose are as follows: 0.1 μ M: 5 wildtype and 6 Akita cells; 1 μ M: 6 wildtype and 9 Akita cells; 10 μ M: 11 wildtype and 15 Akita cells; 100 μ M: 5 wildtype and 5 Akita cells.



Supplemental Figure 9: Effects of CCh on the hyperpolarization-activated current (I_f) in wildtype and Akita SAN myocytes. Representative I_f recordings are shown in control conditions and after application of CCh (10 μ M) in wildtype (A) and Akita (B) SAN cells. The inset shows the voltage clamp protocol. Summary I-V relationships for wildtype (C) and Akita (D) SAN myocytes illustrate that CCh reduced I_f density similarly in both groups of mice. * $P < 0.05$ vs control; $n = 8$ wildtype and 8 Akita SAN myocytes. Data analyzed by paired Student's t -test at each membrane potential.



Supplemental Figure 10: Expression of RGS4 in the sinoatrial node and right atrium of wildtype and Akita mice. (A) RGS4 expression in the SAN and right atrium (RA) in wildtype and Akita mice. $*P < 0.05$ vs. RA within genotype. There were no significant differences in expression of RGS4 between genotypes in the SAN or RA ($P = 0.706$). Data analyzed by two way ANOVA with Tukey's posthoc test; $n = 8$ right atrial samples and 6 SAN samples. (B) mRNA expression of HCN4 and ANP to confirm that samples used in panel A were from the SAN or the right atrium as indicated. Note scale break on Y axis. $*P < 0.05$ vs. right atrium within genotype by two way ANOVA with Tukey's posthoc test.

Supplemental Table 1: Echocardiographic measurements in wildtype and Akita mice.

	WT	Akita
LA diameter (mm)	1.6±0.03	1.7±0.03*
Aortic diameter	1.4±0.01	1.4±0.01
LA/Aorta	1.1±0.02	1.2±0.02*
IVSd (mm)	0.8±0.03	0.9±0.02
IVSs (mm)	1.3±0.02	1.4±0.04
LVPWd (mm)	0.7±0.02	0.7±0.02
LVPWs (mm)	1.2±0.03	1.3±0.03
LVIDd (mm)	3.6±0.1	3.5±0.1
LVIDs (mm)	2.6±0.1	2.1±0.03
EF (%)	71.6±1.1	76.4±1*
FS (%)	35.3±0.7	38.3±0.4*
Heart rate (beats/min)	444±13	403±9*

LA diameter, left atrial diameter; LA/Ao, left atrial-aortic root ratio (indicator of atrial size); IVS, interventricular septum thickness; LVID, left ventricular internal diameter; LVPW, left ventricular posterior wall thickness. IVS, LVID and LVPW measurements are presented during diastole (d) and systole (s). EF, ejection fraction; FS, fractional shortening. Data are means ± SEM; $n=12$ mice in each group. * $P<0.05$ vs. wildtype by Student's t -test.

Supplemental Table 2: Spontaneous AP parameters in wildtype and Akita mice

	wildtype		Akita	
	Baseline	CCh	Baseline	CCh
AP frequency (APs/min)	174±13.7	96±19.8*	164±10.5	136±10.9* ⁺
MDP (mV)	-67.1±0.7	-71.9±1.2*	-67.3±1.0	-69.2±1.3* ⁺
DD slope (mV/s)	38.6±2.8	14.1±3.7*	34.9±3.3	26.8±2.9* ⁺
TOP (mV)	-46.1±1.3	-45.7±1.2	-46.8± 1.5	-46.2±1.1

AP frequency, action potential frequency; MDP, maximum diastolic potential; DD slope, diastolic depolarization slope; TOP, take-off potential. CCh was applied at a dose of 0.1 μ M. * $P<0.05$ vs. baseline; ⁺ $P<0.05$ vs. wildtype. Data analyzed by two way ANOVA with Tukey's posthoc test; $n = 7$ wildtype and 7 Akita SAN myocytes.

References

- [1] Yoshioka M, Kayo T, Ikeda T, Koizumi A. A novel locus, Mody4, distal to D7Mit189 on chromosome 7 determines early-onset NIDDM in nonobese C57BL/6 (Akita) mutant mice. *Diabetes* 1997;46:887-94.
- [2] Kayo T, Koizumi A. Mapping of murine diabetogenic gene mody on chromosome 7 at D7Mit258 and its involvement in pancreatic islet and beta cell development during the perinatal period. *J Clin Invest* 1998;101:2112-8.
- [3] Wang J, Takeuchi T, Tanaka S, Kubo SK, Kayo T, Lu D, et al. A mutation in the insulin 2 gene induces diabetes with severe pancreatic beta-cell dysfunction in the Mody mouse. *J Clin Invest* 1999;103:27-37.
- [4] Hsueh W, Abel ED, Breslow JL, Maeda N, Davis RC, Fisher EA, et al. Recipes for creating animal models of diabetic cardiovascular disease. *Circ Res* 2007;100:1415-27.
- [5] Rose RA, Sellan M, Simpson JA, Izaddoustdar F, Cifelli C, Panama BK, et al. Iron overload decreases CaV1.3-dependent L-type Ca²⁺ currents leading to bradycardia, altered electrical conduction, and atrial fibrillation. *Circ Arrhythm Electrophysiol* 2011;4:733-42.
- [6] Springer J, Azer J, Hua R, Robbins C, Adamczyk A, McBoyle S, et al. The natriuretic peptides BNP and CNP increase heart rate and electrical conduction by stimulating ionic currents in the sinoatrial node and atrial myocardium following activation of guanylyl cyclase-linked natriuretic peptide receptors. *J Mol Cell Cardiol* 2012;52:1122-34.
- [7] Azer J, Hua R, Vella K, Rose RA. Natriuretic peptides regulate heart rate and sinoatrial node function by activating multiple natriuretic peptide receptors. *J Mol Cell Cardiol* 2012;53:715-24.
- [8] Azer J, Hua R, Krishnaswamy PS, Rose RA. Effects of natriuretic peptides on electrical conduction in the sinoatrial node and atrial myocardium of the heart. *J Physiol* 2014;592:1025-45.
- [9] Mangoni ME, Nargeot J. Properties of the hyperpolarization-activated current (I_f) in isolated mouse sino-atrial cells. *Cardiovasc Res* 2001;52:51-64.
- [10] Verheijck EE, van Kempen MJ, Veereschild M, Lurvink J, Jongsma HJ, Bouman LN. Electrophysiological features of the mouse sinoatrial node in relation to connexin distribution. *Cardiovasc Res* 2001;52:40-50.
- [11] Liu J, Dobrzynski H, Yanni J, Boyett MR, Lei M. Organisation of the mouse sinoatrial node: structure and expression of HCN channels. *Cardiovasc Res* 2007;73:729-38.
- [12] Fedorov VV, Chang R, Glukhov AV, KostECKI G, Janks D, Schuessler RB, et al. Complex interactions between the sinoatrial node and atrium during reentrant arrhythmias in the canine heart. *Circulation* 2010;122:782-9.
- [13] Farman GP, Tachampa K, Mateja R, Cazorla O, Lacampagne A, de Tombe PP. Blebbistatin: use as inhibitor of muscle contraction. *Pflugers Arch* 2008;455:995-1005.
- [14] Glukhov AV, Fedorov VV, Anderson ME, Mohler PJ, Efimov IR. Functional anatomy of the murine sinus node: high-resolution optical mapping of ankyrin-B heterozygous mice. *Am J Physiol Heart Circ Physiol* 2010;299:H482-91.
- [15] Fedorov VV, Glukhov AV, Chang R. Conduction barriers and pathways of the sinoatrial pacemaker complex: their role in normal rhythm and atrial arrhythmias. *Am J Physiol Heart Circ Physiol* 2012;302:H1773-83.

- [16] Nygren A, Lomax AE, Giles WR. Heterogeneity of action potential durations in isolated mouse left and right atria recorded using voltage-sensitive dye mapping. *Am J Physiol Heart Circ Physiol* 2004;287:H2634-43.
- [17] Morley GE, Vaidya D, Samie FH, Lo C, Delmar M, Jalife J. Characterization of conduction in the ventricles of normal and heterozygous Cx43 knockout mice using optical mapping. *J Cardiovasc Electrophysiol* 1999;10:1361-75.
- [18] Hua R, Adamczyk A, Robbins C, Ray G, Rose RA. Distinct patterns of constitutive phosphodiesterase activity in mouse sinoatrial node and atrial myocardium. *PLoS One* 2012;7:e47652.
- [19] Rae J, Cooper K, Gates P, Watsky M. Low access resistance perforated patch recordings using amphotericin B. *J Neurosci Methods* 1991;37:15-26.
- [20] Hamill OP, Marty A, Neher E, Sakmann B, Sigworth FJ. Improved patch-clamp techniques for high-resolution current recording from cells and cell-free membrane patches. *Pflugers Arch* 1981;391:85-100.
- [21] Lomax AE, Rose RA, Giles WR. Electrophysiological evidence for a gradient of G protein-gated K⁺ current in adult mouse atria. *Br J Pharmacol* 2003;140:576-84.
- [22] DiFrancesco D, Tromba C. Inhibition of the hyperpolarization-activated current (I_f) induced by acetylcholine in rabbit sino-atrial node myocytes. *J Physiol* 1988;405:477-91.
- [23] Honjo H, Boyett MR, Kodama I, Toyama J. Correlation between electrical activity and the size of rabbit sino-atrial node cells. *J Physiol* 1996;496 (Pt 3):795-808.
- [24] Marionneau C, Couette B, Liu J, Li H, Mangoni ME, Nargeot J, et al. Specific pattern of ionic channel gene expression associated with pacemaker activity in the mouse heart. *J Physiol* 2005;562:223-34.
- [25] Park HJ, Zhang Y, Du C, Welzig CM, Madias C, Aronovitz MJ, et al. Role of SREBP-1 in the development of parasympathetic dysfunction in the hearts of type 1 diabetic Akita mice. *Circ Res* 2009;105:287-94.
- [26] Zhang Y, Welzig CM, Picard KL, Du C, Wang B, Pan JQ, et al. Glycogen synthase kinase-3beta inhibition ameliorates cardiac parasympathetic dysfunction in type 1 diabetic akita mice. *Diabetes* 2014;63:2097-113.